Methods for Evaluating Aquifer-System Parameters from a Cumulative Compaction Record

Amanda J. VanHaitsma

Thesis submitted to the faculty of the Virginia Polytechnic Institute and State University
in partial fulfillment of the requirements for the degree of

Master of Science
In
Geosciences

Thomas J. Burbey, Committee Chair
Madeline E. Schreiber
Pang Du

June 20th, 2016
Blacksburg, VA

Keywords: aquifer-system parameters, compaction, Lorenzi site, Las Vegas, subsidence

Methods for Evaluating Aquifer-System Parameters from a Cumulative Compaction Record

Amanda J. VanHaitsma

ABSTRACT

Although many efforts and strategies have been implemented to reduce over-pumping of aquifer-systems, land subsidence is still a serious issue worldwide. Accurate aquifer characterization is critical to understand the response of an aquifer-system to prolonged pumping but is often difficult and expensive to conduct. The purpose of this thesis is to determine the validity of estimating aquifer-system parameters from a single cumulative compaction record and corresponding nested water-level data deconvolved into temporal components.

Over a decade of compaction and water-level data were collected from an extensometer and multi-level piezometer at the Lorenzi site in Las Vegas Valley and when graphed yearly, seasonal, and daily signals are observed. Each temporal signal reflects different characteristics of the aquifer-system, including the distinction between aquifer and aquitard parameters, as the three temporal stresses influence the compaction record uniquely. Maximum cross-correlation was used to determine the hydrodynamic lag between changing water-levels and subsidence within the seasonal signal while principal components analysis was used to statistically verify the presence of the three temporal signals.

Assumptions had to be made but nearly all estimated Lorenzi site aquifer-system parameters fell either within the reasonable range or were similar in magnitude to parameter values estimated in previous studies. Unfortunately, principal components analysis was unable to detect the three temporal signals. A cumulative compaction record may be difficult to obtain but analyzing the precision measurements of an extensometer results in precise aquifer-system parameters and as the precision of aquifer-system parameters increase so does the ability to sustainably manage groundwater.

Methods for Evaluating Aquifer-System Parameters from a Cumulative Compaction Record

Amanda J. VanHaitsma

GENERAL AUDIENCE ABSTRACT

Although many efforts and strategies have been implemented to reduce over-pumping of aquifer-systems, one of the main causes of land subsidence, land subsidence is still a serious issue worldwide. Accurate aquifer characterization is critical to understand the response of the aquifers and aquitards present to prolonged pumping but is often difficult and expensive to conduct. The purpose of this thesis is to determine the validity of estimating aquifer-system parameters, such as specific storage and hydraulic conductivity, from a single cumulative compaction record and corresponding water-level data from three vertically separated confined aquifers deconvolved into temporal components.

Over a decade of compaction and water-level data were collected from an extensometer and multi-level small diameter observation wells at the Lorenzi site in Las Vegas Valley and when graphed yearly, seasonal, and daily signals are observed. Each temporal signal reflects different characteristics of the aquifer-system, including the distinction between aquifer and aquitard parameters, as the three temporal stresses influence the compaction record uniquely. Maximum cross-correlation was used to determine the hydrodynamic time lag between changing water-levels and subsidence within the seasonal signal while principal components analysis was used to statistically verify the presence of the three temporal signals.

Assumptions had to be made but nearly all estimated Lorenzi site aquifer-system parameters either fell within the reasonable range or were similar in magnitude to parameter values estimated in previous studies. Unfortunately, principal components analysis was unable to detect the three temporal signals. A cumulative compaction record may be difficult to obtain but analyzing the precision measurements of an extensometer results in precise aquifer-system parameters and as the precision of aquifer-system parameters increase so does the ability to sustainably manage groundwater.

ACKNOWLEDGEMENTS

I would like to acknowledge the National Science Foundation and the Virginia Tech Geoscience Department for providing funding for this research.

My deepest gratitude goes to my committee members for their patient guidance, enthusiastic encouragement, and for always being available.

I also wish to thank my family and friends for their love and support throughout my study.

TABLE OF CONTENTS

LIST OF FIGURES

LIST OF TABLES

CHAPTER 1: INTRODUCTION

Land subsidence refers to the lowering of Earth's land surface caused by movements of subsurface materials (UNESCO, 2016). Although there are many causes of subsidence over 80 percent of the 17,000 square miles of the United States that has experienced land subsidence is due to groundwater pumping (USGS, 2013). Damages caused by land subsidence ranges from displaced roads and house foundations to ruptured sewer, water, and gas lines to the creation of earth fissures, or cracks at or near Earth's surface, and increased likelihood of flooding (Bell, 1991). The National Research Council estimated in 1991 that the United States' annual cost for dealing with associated flooding and damages caused by land subsidence was greater than $125 million (USGS, 2013).

Another effect of land subsidence is the loss of storage capacity in aquifer-systems, or the subterranean saturated material that can store, transmit, and yield significant amounts of water (Bell, 1991). Storage capacity refers to the physical space available for storing groundwater and is dependent on the hydrogeologic makeup of the aquifer-system (Bell, 1981). Storage capacity is lowered by the aquifer-system compressing resulting in the actual compaction of aquifer-system materials, or loss of porosity, thus reducing the space available for groundwater storage (USGS, 2013). The loss of storage capacity is of greatest concern for many areas of the arid southwest, such as Las Vegas, Nevada.

As one of the fastest growing metropolitan areas Las Vegas, Nevada (Figure 1) has experienced increased demands for water resources, resulting in groundwater withdrawals from the aquifer-system within Las Vegas Valley that have exceed the estimated natural recharge into the basin beginning in the 1950's (Malmberg, 1965). By the 1990's continued groundwater exploitation far exceeding natural recharge resulted in groundwater levels declines of more than

91 m (Burbey, 1995) causing aquifer-system compaction, land subsidence, and earth fissuring to occur (Maxey and Jameson, 1948; Malmberg, 1965; Bell, 1981). However, water management practices, including artificial recharge of the aquifer-system, were also implemented during the 1980s (Bell et al., 2002). In 1994 instrumentation at the Lorenzi site was put in place to study the land subsidence occurring in Las Vegas Valley by the U.S. Geological Survey (USGS) in cooperation with the Nevada Department of Conservation and Natural Resources, Division of Water Resources and the Las Vegas Valley Water District (LVVWD) (Pavelko, 2000). The instrumentation included a high precision pipe extensometer and a nest of three piezometers.

Water management is the best defense against, and deterrent of, land subsidence but it requires information about site-specific aquifer-systems, which can be costly and time consuming to obtain. Hydraulic conductivity, defined as the ability of material to transmit water, and skeletal specific storage, the volume of water that can be released from a unit volume of aquifer for a unit decrease in groundwater level, are two properties of the aquifer-system that can currently be determined for aquifers using on-site aquifer tests (Freeze and Cherry, 1979). Additional piezometers would need to be installed within the confining units coupled with laboratory experiments performed on the aquitard to obtain the same hydraulic parameters for the aquitards as is commonly done for aquifers. Currently the amount of work and cost required to estimate aquifer-system parameters (both aquifers and aquitards) is too great for many aquifer-systems to be adequately understood.

1.1 PURPOSE AND SCOPE

The purpose of this thesis is to determine the validity of estimating aquifer-system parameters from a single cumulative compaction record and corresponding nested water-level data deconvolved into temporal components. The data records used were collected at the Lorenzi

site in northwest Las Vegas, Nevada (Figure 1) from November, 1994 to December, 2007 and consists of hourly total compaction values as well as depth to water-levels for the three vertically separate confined aquifers located at the site. Daily, seasonal, and decadal signals can be observed from the total record and are used to estimate aquifer horizontal hydraulic conductivity and elastic skeletal specific storage as well as the vertical hydraulic conductivity and elastic/inelastic skeletal specific storage of the intervening aquitards (Table 1).

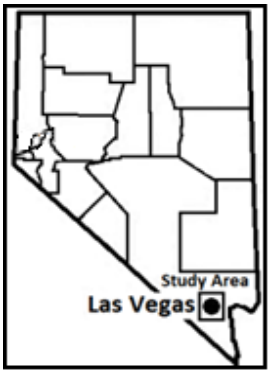

Figure 1: Location of Las Vegas, Nevada (modified from Bell et al., 2002).

Table 1: Aquifer-system parameters estimated from the three temporal signals (daily, seasonal, and decadal signal) deconvolved from the total subsidence record and the analytical method used.

Aquifer-System Unit	Temporal Signal	Parameters Found	Analysis Method
Aquifer	Daily	Elastic specific storage Horizontal hydraulic conductivity	Daily pumping test: Hantush-Jacob (Walton), Hantush-Storage in Aquitard methods
Aquitard	Seasonal	Elastic specific storage	Stress-strain plots
		Vertical hydraulic conductivity	Aquitard-drainage model time constant equation
	Decadal	Inelastic specific storage	Stress-strain plot

1.1.1 Las Vegas Valley Land Subsidence History

In Las Vegas Valley localized aquifer-system compaction and resulting land subsidence can be traced back to decades of groundwater pumping at rates that far exceed the natural recharge into the basin. Over 91 m of groundwater declines and nearly 2 m of land subsidence have occurred since the 1930's (Pavelko, 2000). By the 1970's damage caused by land subsidence and associated earth fissuring became evident on engineered structures, such as buildings, roads, and pipelines (Bell, 1981; Bell and Price, 1993; Bell, 1997). To meet the increasing municipal and domestic water-supply demand in the rapidly growing Las Vegas metropolitan area, additional water was imported from the Colorado River beginning in 1972 (Bell et al., 2002).

By 1987 a seasonal artificial recharge program was initiated by the LVVWD to temporarily store excess Colorado River water in the aquifer-system during the period of low-

water use (winter) in order to slow the compaction rate of the aquifer-system by increasing the groundwater levels and subsequently reducing the effective stress on the aquifer-system (Pavelko, 2000). The seasonal artificial recharge has stabilized and even raised water levels in many parts of the basin thereby lessening land subsidence rates and even resulting in uplift in the northeast and central parts of the valley, but the subsidence record at Lorenzi in the northwest part of the basin still shows a long-term residual compaction trend (Pavelko, 2000).

Four localized subsidence bowls have been defined within a larger valley-wide subsidence bowl (Figure 2) using benchmark and GPS surveys along with interferometric synthetic aperture radar (InSAR) data (Galloway et al., 2000) obtained for the period 1992-97 (Amelung et al., 1999; Bell et al., 2000 and 2002; Hoffmann et al., 2001). In the northwest region of the valley, the deepest localized subsidence bowl has settled 2 m since 1935 (Bell, 1981; Bell et al., 2000). Between 1963 and 1998 the other localized bowls have subsided from 0.7 - 1 m, however, the maximum subsidence regions do not necessary match up with areas of maximum head declines (Bell et al., 2000). In 1993, Bell and Price theorized that the regions with higher subsidence rates were underlain with thicker layers of compressible fine-grained sediments compared to the regions with lower subsidence rates as the cause of discrepancy between maximum subsidence and maximum head decline.

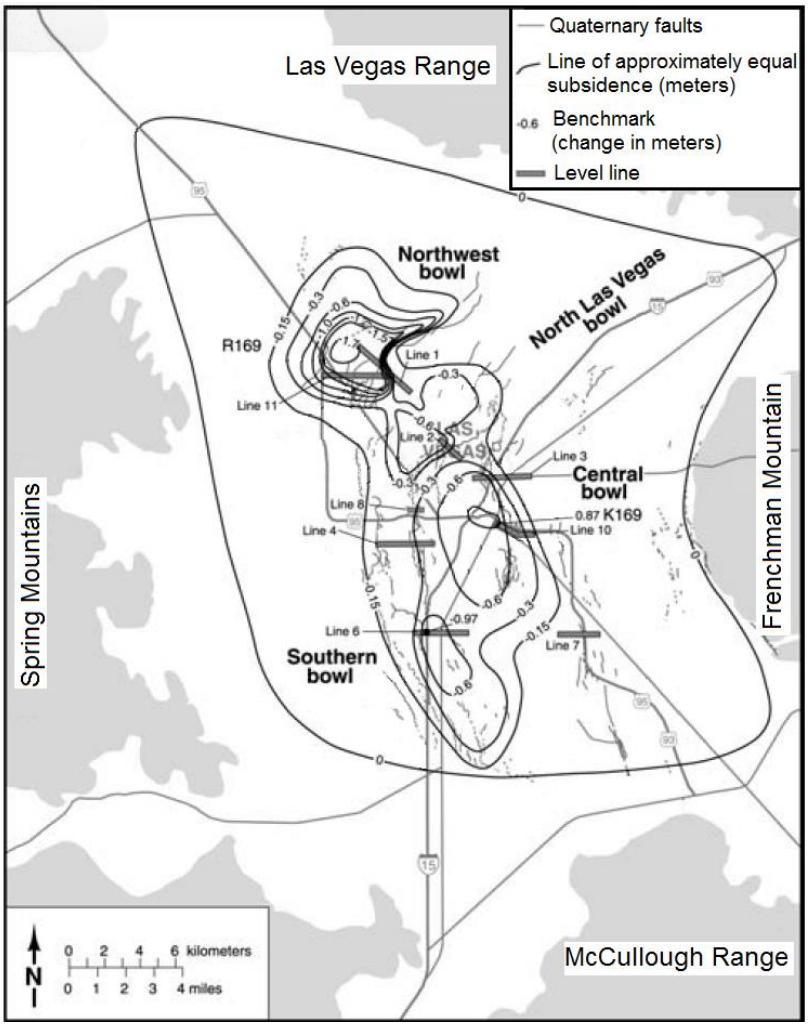

Figure 2: Subsidence map for 1963-2000 showing four localized subsidence bowls within larger regional subsidence bowl (modified from Bell et al., 2002).

1.1.2 Previous Investigations

Water-resources investigations focused on land subsidence and related issues in Las Vegas Valley were examined by Malmberg (1964), Minding (1965, 1971), Bell (1981), Bell and Price (1993), Pavelko and others (1999), and Pavelko (2000). Broad water-resources investigations that include information on land subsidence in Las Vegas Valley include Maxey and Jameson (1948), Domenico and others (1964), Malmberg (1965), and Plume (1989).

Domenico and others (1966) and Burbey (2002) studied geologic controls of land subsidence in Las Vegas Valley while Harrill (1976) studied groundwater storage depletion. Carpenter (1915) worked on general hydrologic investigations of Las Vegas Valley.

Las Vegas Valley groundwater flow and land subsidence was first simulated by Morgan and Dettinger (1996) using a modified version of the Trescott, Pinder, and Larson flow model (the predecessor to MODFLOW). Waichler and Conchran (1991) simulated past and future land subsidence for two sites in Las Vegas Valley using the COMPAC model (Helm, 1975). Jeng (1998) simulated groundwater flow and land subsidence by converting the model of Morgan and Dettinger (1996) to MODFLOW and using the IBS package (Leake and Prudic, 1991) for simulating one-dimensional compaction. Yan (2007) simulated groundwater flow and land subsidence for Las Vegas Valley using the more accurate SUB package (ref) for delayed drainage of interbeds.

Zheng and Burbey (2016, in press) developed a more comprehensive groundwater management model for Las Vegas Valley by modeling a more finely discretized flow and subsidence model where the parameter estimates were inversely determined by taking advantage of water-level and InSAR surface deformation observations to more precisely estimate storage and hydraulic conductivity parameters as well as fault transmissivity. Okyuan (2000) selected specific sites in Las Vegas Valley to simulate past and future land subsidence and rebound associated with recovering water-levels. Sneed and others (2000), Pavelko (2003), and Pavelko (2004) presented preliminary model results for a one-dimensional numerical model of vertical aquifer-system deformation for the Lorenzi site. These one-dimensional models were limited to estimates of elastic and inelastic storage only.

1.2 HYDROGEOLOGY

The hydrogeology of Las Vegas Valley, Nevada was described in detail by Bell in 1981 and only pertinent descriptions of geology and hydrogeology relevant to the objectives of this investigation are provided here.

1.2.1 Geologic Setting

Las Vegas Valley is a structural basin containing hundreds of meters of Pliocene through Holocene aged unconsolidated sediments (Bell et al., 2002). The valley is bounded on the west by the Spring Mountains; to the north by the Desert, Sheep, and Las Vegas Ranges; to the east by the Frenchman and Sunrise Mountains; and to the south by the River Mountains and the McCullough Range (Figure 3). The mountain ranges to the east, west, and north sides of the basin are primarily composed of Paleozoic and Mesozoic sedimentary rocks such as limestones, siltstones, and sandstones. The mountains to the south and southeast however are primarily composed of Tertiary volcanic rocks such as basalts, andesites, and rhyolites resulting in a boundary separating very different geologic conditions lying directly beneath Las Vegas Valley.

Dominated by an old, flat surface the center of the Las Vegas Valley basin represents a previous depositional level with an elevation around 610 m. The Las Vegas Wash extends the length of the northwest-southeast trending valley and is the main drainage with several large tributary drainages flowing into the wash from the northeast, west and southeast. North to northeast trending, east dipping Quaternary fault scarps, as high as 50 m, transect the valley floor, which is bounded on all sides by alluvial fans from the surrounding mountain ranges (Bell et al., 2002).

The geologic history of the region is connected to uplift, igneous activity, and repeated periods of deposition and erosion involved in the development of the Basin and Range province.

The general geologic history of Las Vegas Valley is shown in the stratigraphic column in Table 2. The Paleozoic and Mesozoic eras were dominated by thick depositions of marine sediment, occasionally disturbed by orogenic activity. Sedimentary depositions continued through the Cenozoic but the earlier period of the era was subjected to widespread volcanism and fault activity. From the Miocene, after the peak tectonic activity, through the Quaternary a thick sedimentary section accumulated in the structural basin. This sequence of terrestrial sediments is responsible for most or all of the measured subsidence occurring in the valley today.

The Horse Spring and Thumb Formations, Muddy Creek Formation, and Plio-Pleistocene basin fill make up the Miocene through Quaternary sedimentary section. The Horse Spring and Thumb Formations are the earliest deposits of accumulated sediment with considerable outcrops within the Frenchman Mountain area and a composition composed primarily of limestone, siltstone, sandstone, and conglomerate. The Muddy Creek Formation also outcrops extensively within the Frenchman Mountain and Las Vegas Wash areas and is composed primarily of siltstone, claystone, and sandstone and generally acts as a confining unit or barrier to groundwater flow. Fine-grained facies are more common but coarse-grained Muddy Creek Formation facies become more pronounced closer to the mountains at the basin margin.

The Muddy Creek Formation is found in surface exposures to be flat lying or gently tilted. The top of the formation is between 150 to 300 m below land surface and as a result of erosion, or structural deformation, is found to be irregular. Subsurface thicknesses are inferred to be hundreds of meters thick but are highly interpretive due to the lack of direct data. The Muddy Creek Formation has been cut by many small faults and locally sheared and tilted in the Las Vegas Wash area. The formation is not found west of Las Vegas and has a sharp fault contact with the Frenchman Mountain. The placement and magnitude of features related to subsidence in

the Las Vegas Valley basin are primarily controlled by the Muddy Creek Formation along with the Plio-Pleistocene basin fill and the hydrologic setting of the basin.

As much as 300 m of Pliocene to Pleistocene aged sediment makes up the Plio-Pleistocene basin fill with an unknown unconformity present between the Muddy Creek Formation and the basin fill. The Plio-Pleistocene basin fill can be broken down into three facies; coarse-grained, fine-grained, and blue clay. The coarse-grained alluvium is composed of poorly sorted sand and gravel while the fine-grained alluvium has more silts and sandy silts. The coarse-grained facies flanks the surrounding mountain ranges with the fine-grained facies localized in the center of the basin.

Most of the fine-grained alluvium can be found as well-cemented, essentially impermeable caliche randomly distributed as horizons of up to a meter thick. Also located in the center of the basin is the blue clay facies, usually occurring at depths of 115 to 137 m below land surface. The subsurface cross section (Figure 5) shows a gradual lateral grading of a thick sand and gravel alluvial wedge from the Spring Mountains to fine-grained silts and clays toward the center of the basin. The entire basin margin exhibits a similar lateral inter-fingering although on a slightly smaller scale.

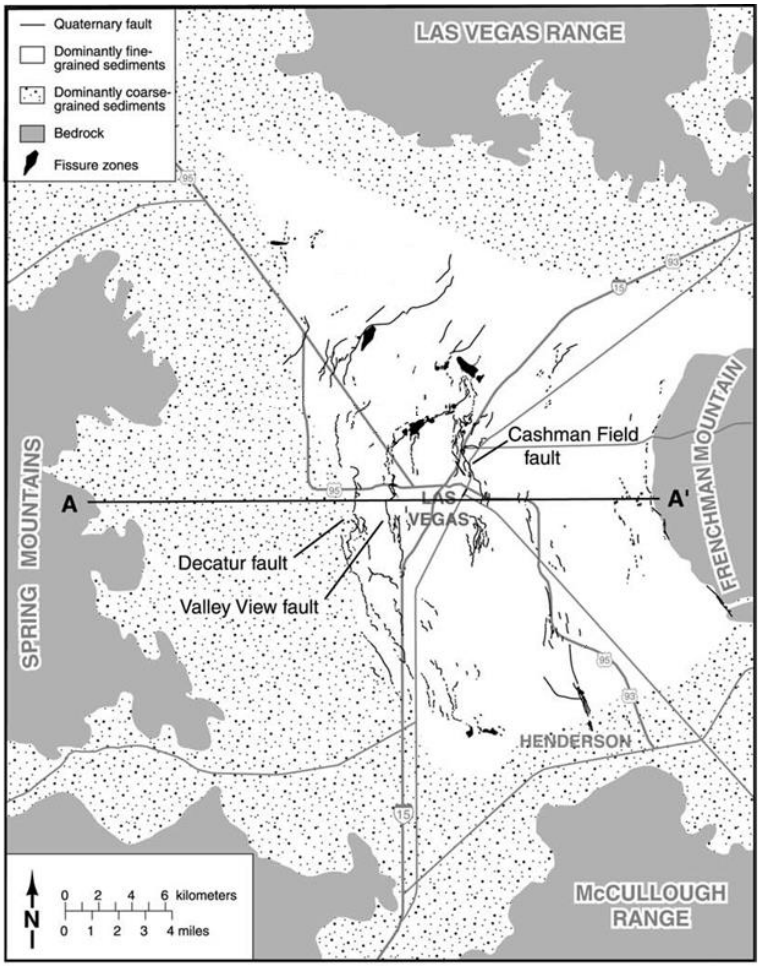

Figure 3: Las Vegas Valley, Las Vegas, Nevada generalized surface geology map displaying fissure zones and Cashman Field, Decator, and Valley View faults. Line A-A' indicates geologic cross-section location (modified from Bell et al., 2002).

Table 2: Generalized geologic history of Las Vegas Valley, Las Vegas, Nevada showing stratigraphy with corresponding age (adapted from Bell, 1981).

Geologic unit in Las Vegas area	Epoch	Period	Era	Age before present (millions of years)
Recent alluvium	Holocene	Quaternary	Cenozoic	0.01
Plio-Pleistocene Basin Fill	Pleistocene			1.8
Muddy Creek Fm	Pliocene	Tertiary		5.2
Horse Spring Fm Thumb Fm	Miocene			22.5
Intrusive (igneous), extrusive (volcanic), and sedimentary (continental limestone, sandstone, shale) rocks	Pre-Miocene			65
Sedimentary rocks (marine); dominantly sandstones and limestones			Mesozoic	225
Sedimentary rocks (marine); dominantly carbonate rocks with sandstone			Paleozoic	570
Igneous and metamorphic “basement” rocks			Precambrian	

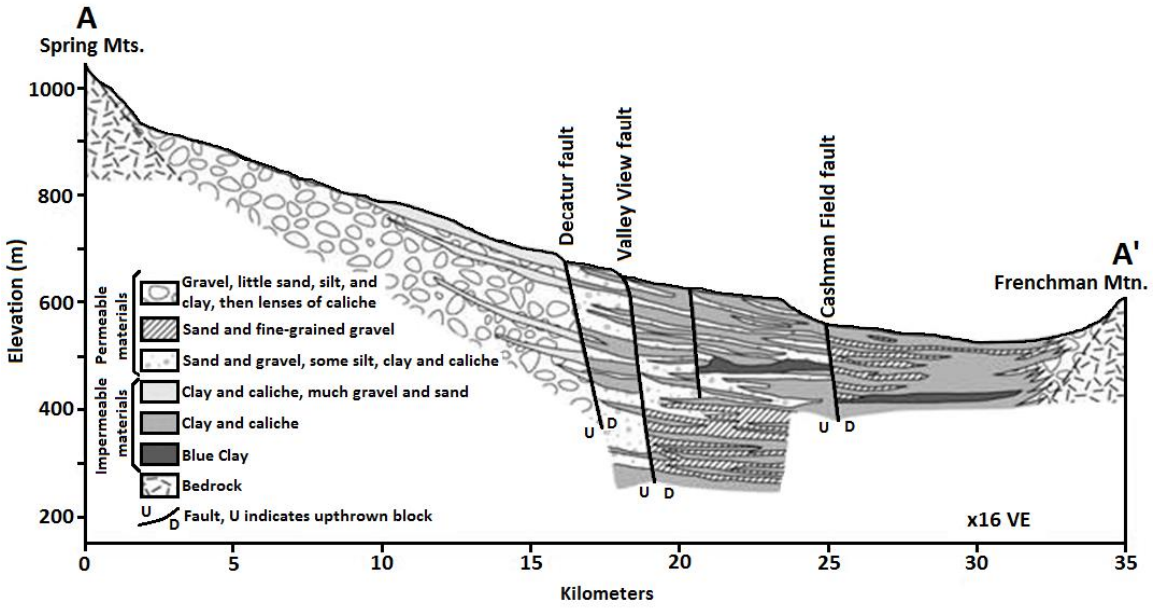

Figure 4: Geologic cross-section showing the allotment of coarse and fine-grained deposits and fault interactions inferred from well logs (modified from Bell et al., 2002).

1.2.2 Hydrogeologic Setting

Groundwater is generally pumped from the upper 600 m of the aquifer-system which is composed of the Muddy Creek Formation and overlying Plio-Pleistocene basin fill sediments (Pavelko, 2004). Maxey and Jameson (1948) originally subdivided the aquifer-system into two major sections; the Near-Surface Water and the Confined Water, which later became known as the Principal Aquifer. In most places, although absent from the western part of Las Vegas Valley, the first water encountered during drilling is the Near-Surface Water which can be found under confined or unconfined groundwater conditions (Pavelko, 2000). Very little groundwater is pumped from the 30 – 90 m thick Near-Surface Water aquifer-system section since the main source of its recharge has become industrial and irrigation waters as well as infiltration from sewage and secondary recharge from lawn and golf course watering. The Principal Aquifer, with

its confined and semi-confined conditions, underlies the Near-Surface Water and is the primary source of groundwater for Las Vegas Valley (Pavelko, 2000).

The Principal Aquifer extends from the margins of Las Vegas Valley, where sand and gravels dominate, becoming less common and more discontinuous towards the eastern and central parts of the valley do to the increase in the percentage of clays and silts (Pavelko, 2004). The Principal Aquifer is subdivided into shallow, middle, and deep zones based on the presence of aquitards created by numerous thin, impermeable caliche and clay horizons (Pavelko, 2004). The shallow zone is found at depths of as much as 90 m, immediately below the Near-Surface Water, and is underlain by Plio-Pleistocene blue clay horizons. Between the blue clay horizons and the base of the Plio-Pleistocene basin fill, and made up of several random permeable sand and gravel layers is the middle zone. Beneath the middle zone lies the Muddy Creek Formation with sediments containing large quantities of water but with small transmissivities the sediments do not yield water readily. Gravel layers present within the Muddy Creek Formation make up the deep zone.

Harrill (1976) determined that the primary recharge of the Principal Aquifer comes in through lateral recharge from the mountain blocks primarily from the west, although infiltration of surplus surface water could create some local secondary recharge. Originally, Maxey and Jameson (1948) estimated natural recharge entering the Las Vegas Valley aquifer-system from precipitation, largely originating in the Spring Mountains, to be around 31 to 43 $\frac{hm^3}{yr}$. However, an alternative altitude-precipitation relationship implemented in a study by Donovan and Katzer (2000) suggested a net annual natural recharge in the range of 62 to 70 $\frac{hm^3}{yr}$. Before 1962 many springs and seeps found throughout the Las Vegas Valley floor used to discharge under natural

conditions however, groundwater pumping lowered water levels significantly enough that spring flow has effectively ceased.

1.3 LORENZI SITE

The Lorenzi site is located at the Nevada Power Company's Lorenzi substation in northwestern Las Vegas, Nevada on Rainbow Boulevard between Alexander and Craig Roads (Figure 5). Higher rates of land subsidence within the surrounding area, particularly toward the north, along with an accessible and protected location from vandalism lead to the Lorenzi site selection located within a two-mile radius of 14 LVVWD wells in 1994 (Harrill, 1976; Bell, 1981). The LVVWD wells are used for seasonal groundwater pumping, from May through September, as well as for artificial recharge from October to April (Pavelko, 2000). LVVWD wells AR010 and AR094 (Figure 5) are only used for artificial recharge while wells 69, 88, 92, 94, 101, 103, 116, and 117 (Figure 5) are used only for groundwater pumping, and wells 28, 29, 33, and 72 (Figure 5) are used to both pump groundwater and artificially recharge the aquifer system (Pavelko, 2000).

The Lorenzi site contains a 244 m deep vertical borehole extensometer (EXT1) and three nested piezometers with casing depths at 97.5, 142, and 212 m below land surface (PZS, PZM, and PZD respectively). Geophysical logs, taken within the extensometer borehole, indicate the presence of three confined aquifers at depth ranges of 69 to 94, 128 to 152, and 184 to 244 meters below land surface (F.L. Paillet, U.S. Geological Survey written commun., 1994, as cited in Pavelko, 2000). A lithologic log, also taken from the extensometer borehole, reveals sand and gravel aquifers with silt and clay interbedded layers and silt and clay dominated aquitards (T.J. Burbey, U.S. Geological Survey written commun., 1994, as cited in Pavelko, 2000). Pavelko, in

2000, prepared a USGS report that described the layout of the Lorenzi site and is reiterated in the following Piezometer and Site Set Up and Extensometer System subsections.

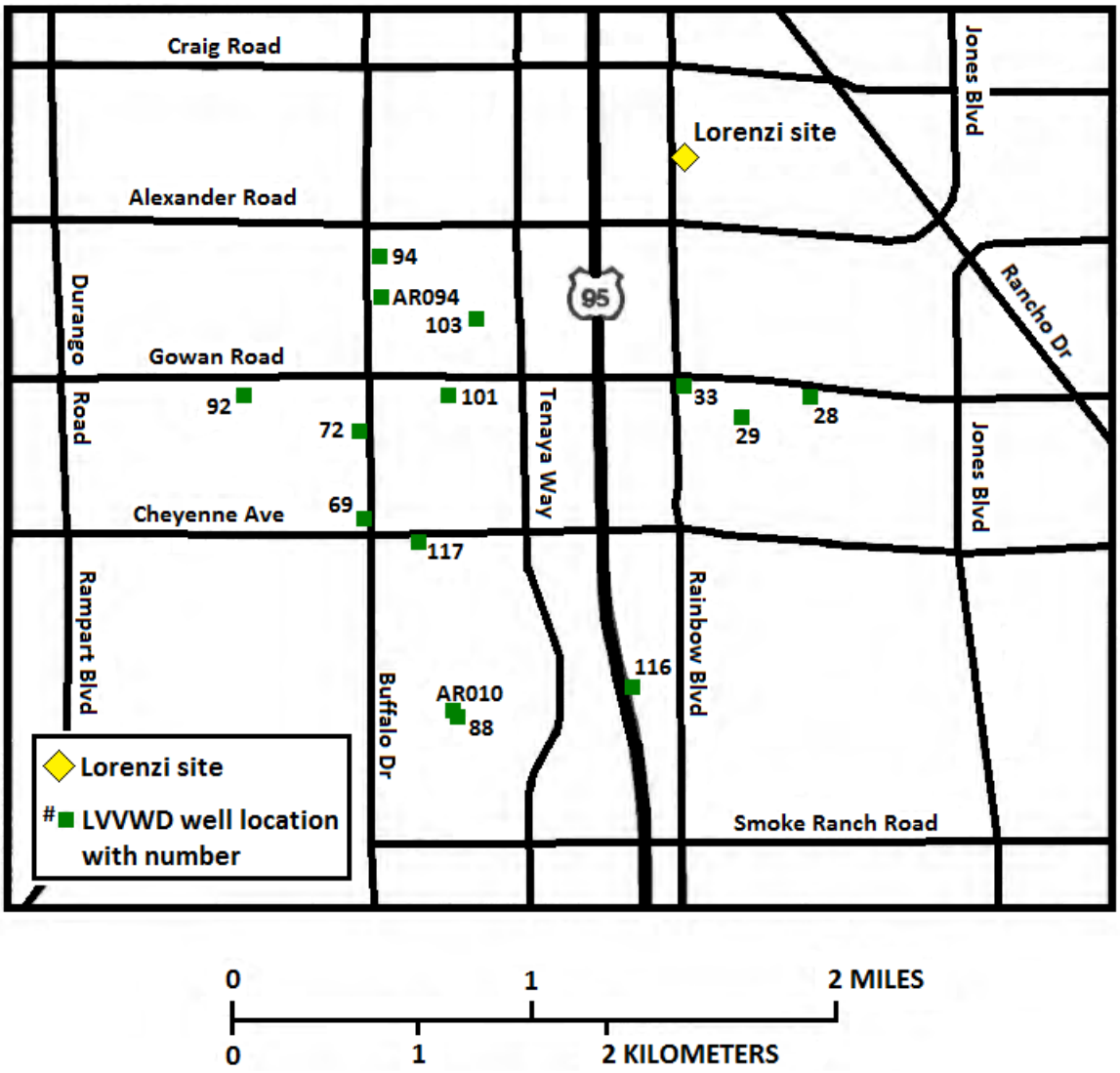

Figure 5: Location of Lorenzi site as well as 14 Las Vegas Valley Water District (LVVWD) wells in Las Vegas Valley, Las Vegas, Nevada (modified from Pavelko, 2000).

1.3.1 Piezometer and Site Set Up

A small housing unit protects the nested piezometers while a separate wooden shed houses the extensometer roughly 6 m from the piezometers. A barometer, data logger, data storage device, electronics-panel box to incase the logger and storage device, and air-temperature probes are also housed within the wooden shed. Air temperature is measured inside the electronics-panel box and wooden shed, as well as within the extensometer borehole 3 m below the land surface in order to evaluate the potential impacts that temperature has on the extensometer record due to thermal expansion and contraction of the metal components of the extensometer system due to changing temperatures. Barometric pressure is also measured and recorded at the site. The power for the data logger and storage device comes from a rechargeable battery for which voltage is conditioned by a voltage regulator from a solar panel that provides all necessary power year round.

Installation for the three nested piezometers occurred in May 1994 at the Lorenzi site. A 0.41 m diameter borehole was drilled to allow for the 0.30 m steel surface conductor casing. The steel conductor casing extends to a depth of approximately 16 m. A 0.31 m diameter borehole was subsequently drilled from 16 to 214 m below land surface. PZS and PZM are fashioned from 0.05 diameter polyvinyl chloride (PVC) casings and screens while PZD is fashioned from 0.06 m outer diameter acrylonitrile butadiene styrene (ABS) casing and screen. The PZD had internal vertical grooves that allowed for a borehole inclinometer to be employed for measurements of tilt and deviation (Burbey, 2005). Each of the three piezometers is screened at a below land surface depth interval consistent with the geophysical log identified as an aquifer: PZS from 91 to 94 m, PZM from 136 to 139 m, and PZD from 206 to 209 m. The annular space flanking each screened interval is filled with gravel pack with the remaining annual space filled with neat cement to

isolate each screened interval from other aquifer system zones. Table 3 lists all construction data for each piezometer and Figure 6 shows each construction.

Water-level data were collected hourly using pressure transducers from November 2004 to December 2007 with occasional steel tape measurements made to calibrate the transducers. The PZS and PZM transducers had a pressure range of 0 - 30 $\frac{lbs}{in^2}$ while the PZD transducer had a range of 0 - 50 $\frac{lbs}{in^2}$. The depth to water-levels are reported to 0.01 ft after being converted. Each transducer was vented at the land surface to minimize atmospheric pressure changes that could affect pressure measurements. A barometric pressure sensor, with a range of 800 – 1100 millibars, measured barometric pressure at the site.

Table 3: Extensometer and three piezometer well-construction data, located at Lorenzi site, Las Vegas, Nevada (adapted from Pavelko, 2000).

Well Name	Date Drilled (1994)	Depth	Casing depth	Top of screened interval	Bottom of screened interval
		Meters below land-surface			
PZD	May 18	214	212	206	209
PZM	May 18	214	142	136	139
PZS	May 18	214	97.5	91	94.5
EXT1	April 3	244	238	--	--

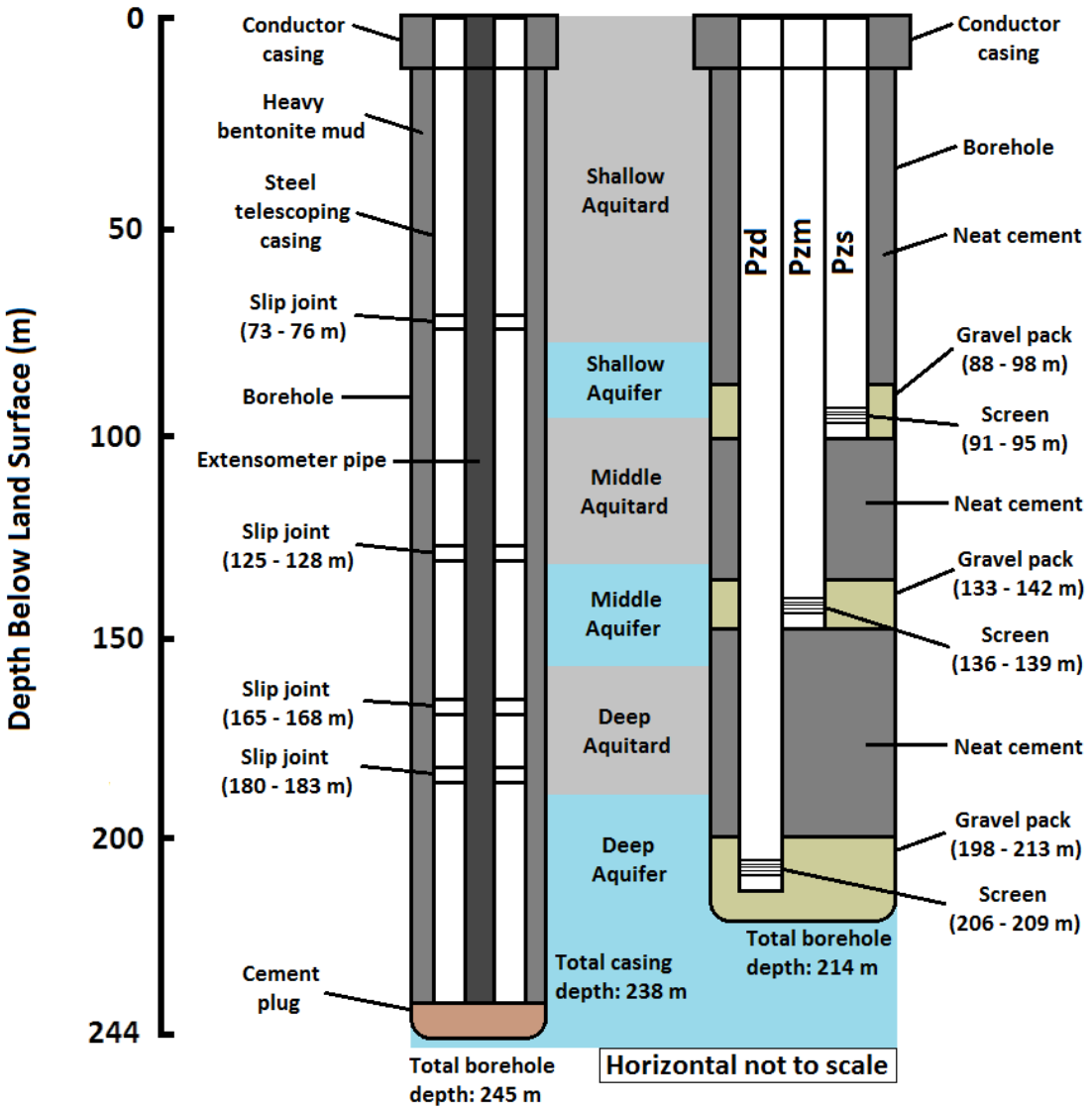

Figure 6: Piezometer and extensometer underground construction at Lorenzi site, Las Vegas, Nevada (adapted from Pavelko, 2000).

1.3.2 Extensometer System

The counterbalance double-pipe extensometer (Figure 6) was installed in April 1994 to measure vertical aquifer-system compaction at the Lorenzi site. To a depth of 16 m a 0.41 m diameter borehole was drilled while a 0.27 m diameter borehole was drilled from 16 to 244 m below land surface. The borehole deviates about 1.75 degrees from vertical according to vertical-

deviation logs created at the time of drilling. Extending down 16 m below land surface is a 0.30 diameter steel conductor casing but a 0.15 diameter steel "telescoping" casing extends the length of the borehole and is affixed within a cement plug at the bottom. During vertical deformation slip joints within the telescoping casing allow the casing string to stretch and contract as needed.

There are four 3 m long slip joints within the telescoping casing. Casing distortion and failure connected to aquifer-system compaction can be delayed by the presence of slip joints within extensometer casing strings, which minimize the frictional stress between the casing and neighboring sediments (Riley, 1986). Down to 16 m below land surface cement occupies the annular space around the conductor casing while heavy bentonite mud fills the annual space around the length of the telescoping casing. Located within the telescoping casing is a 0.05 diameter Schedule 80 steel extensometer pipe that rests 238 m below land surface at the bottom of the borehole on a cement plug.

A steel extensometer table held by two steel table legs sheathed in PVC and secured 3.6 m below land surface sits over the extensometer borehole. To help reduce the effects of shallow sediment deformation, caused by changes in soil temperature or moisture content, the legs of the table are anchored, but not in connection with the neighboring soil. The degree of movement of the table in relation to the extensometer pipe expresses the vertical deformation (compaction or expansion) of the aquifer-system. A linear potentiometer, a dial gage, and an analog chart recorder all record the movement of the table. The linear potentiometer is attached to both the top of the extensometer pipe and the extensometer table while the dial gage is connected to a reference surface attached to the extensometer pipe and the extensometer table. The analog chart recorder uses a counterweighted pulley system to connect to the extensometer pipe and sits on the extensometer table.

To reduce flexing of the extensometer pipe so that friction against the outer steel casing is minimized in the borehole, the weight of the pipe is supported by an above ground counterbalance with steel weights using an asymmetric lever system. An asymmetric lever system is used to reduce the weight of the steel counterbalance required to support the extensometer pipe. The mechanical advantaged achieved is 8:1. To further minimize flexing of the extensometer pipe, and to keep the pipe in line with the recording instruments, the asymmetric lever arm is kept level. Degradation of the extensometer data can occur if the pipe flexes and causes friction between the steel casing and extensometer pipe (Riley, 1986). Additional frictional-stress relations can occur as the result of a bowed extensometer pipe or an off-vertical casing (Riley, 1986).

A dead-band test is used to determine the model counterbalance weight, establish the frictional properties of the extensometer, gain understanding of the extensometer general performance, and test the reliability of the recordings. A dead-band test addresses the capability of an extensometer to restore the lever arm to a neutral starting position after the addition and removal of a counterbalance weight. Each counterbalance weight could have its own dead-band which is the distance between the starting and ending positions for one counterbalance weight.

Usually, the smallest dead-band indicates the best counterbalance weight for the extensometer (D.L. Galloway, U.S. Geological Survey oral commun., 2000, as cited in Pavelko, 2000). The smallest dead-band for EXT1 was the result of a 250 lbs. counterbalance weight. Over time most extensometers are subjected to data degradation do to the impossibility of completely removing frictional stresses. One visible result of frictional stresses on extensometer data is “Stick-slips,” which are step-wise jumps seen in data created by the sudden release of accumulated frictional pressure (Riley, 1986).

The primary measuring device at the Lorenzi site for the monitored aquifer-system compaction was a digital linear potentiometer. The linear potentiometer outputs the compaction as changes in millivolts, which was later converted to compaction by a linear relation determined from calibration data. Compaction was reported to 1.0^{-4} in and recorded every hour on an electronic data logger. An analog chart recorder provided a backup continuous record of compaction data. Since the first day of record, November 16, 1994, the compaction data had been cumulatively measured until December, 2007. The aquifer-system compaction measured is between the depths of the bottom of the extensometer table, 3.7 m below land surface, and the bottom of the borehole extensometer, 244 m below land surface.

1.4 ANALYTICAL APPROACH

1.4.1 Aquitard Drainage Model

Most theoretical methods used to predict land subsidence, resulting from groundwater withdrawal, are conceptually based on the aquitard drainage model. The core concepts comprising the aquitard drainage model are the principle of effective stress and the theory of hydrodynamic consolidation (Holzer, 1998). The aquitard drainage model states that the irreversible compaction of slow draining aquitards, explained by the principle of effective stress and the theory of hydrodynamic consolidation, accounts for nearly all of the permanent land subsidence that occurs due to groundwater withdrawal (Tolman and Poland, 1940). Before the suggestion of the aquitard drainage model declining head levels and the subsequent compaction of permeable sands were thought to be the primary factor leading to land subsidence (Holzer, 1998).

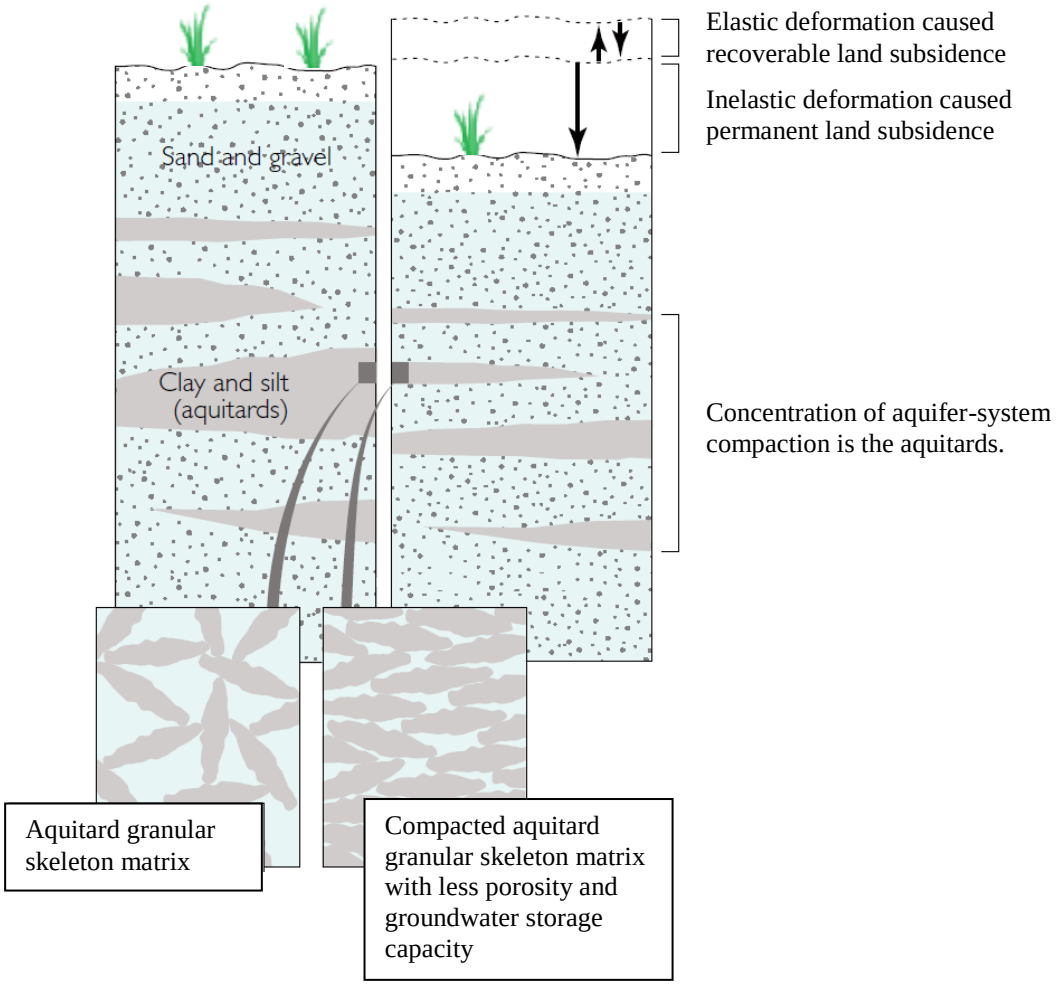

Figure 7: Stresses on aquitards, larger than the past preconsolidation stress, due to long-term pumping result in permanent aquitard compaction and land subsidence. Aquitard compaction due to stresses smaller than the past preconsolidation stress results in elastic aquitard compaction (modified from USGS, 1999).

1.4.2 Principle of Effective Stress

Terzaghi's principle of effective stress (1925, 1943) explains the relationship between vertical aquifer-system deformation and fluctuating head levels, which can be expressed in terms of fluid pressures. A confined aquifer, or confining unit, can be thought to contain an imaginary plane on which a total stress (σ_T), the weight of overlying sediments, atmosphere, and water, is acting (Figure 7). The principle of effective stress states that fluid pressure (p), from the pore

spaces between grains, and the effective stress (σ_e), from the granular matrix, beneath the imaginary plane support the total stress acting from above:

$$\sigma_T = p + \sigma_e$$

Total stress (σ_T) can be assumed to remain constant for a confined aquifer-system that does not have a water-table aquifer, like the Lorenzi Site. With a constant total stress (σ_T) any change in fluid pressure (p), or head level, will result in an equal and opposite change in effective stress (σ_e) within the aquifer-system. The change in effective stress (σ_e) is what can cause aquifer-system deformation. When water is pumped from a confined aquifer the head levels, or fluid pressures (p), decrease and cause an equal and opposite increase in the effective stress (σ_e) that when large enough can result in aquifer-system compaction. The amount of aquifer-system compaction that occurs depends, in part, on the sediment compressibilities and the stress history of the system.

The relationship between an aquifer-system's current effective stress (σ_e) to the previous maximum effective stress, also known as preconsolidation stress ($\sigma_{e(\max)}$), will determine if the deformation that occurs is recoverable or permanent since aquifer-system sediments have an elastic and inelastic compressibility. As long as the preconsolidation stress ($\sigma_{e(\max)}$) remains larger than the current effective stress (σ_e) any aquifer-system deformation will be recoverable (elastic). When head levels drop low enough, usually below the previous minimum head level, the preconsolidation stress ($\sigma_{e(\max)}$) is exceeded and the aquitard granular matrix experiences permanent rearrangement resulting in a reduction in pore volume (inelastic). The storage capacity (S) of the aquifer-system is permanently reduced from this one-time release of stored aquitard groundwater.

Elastic and inelastic sediment compressibilities, known as skeletal compressibilities, can be expressed as skeletal specific storages (S_{sk}). A skeletal specific storage (S_{sk}) is the product of the sediment's compressibility (α_k), the density of water (ρ), and gravitational acceleration (g):

$$\left.\begin{aligned} S_{ske} &= \alpha_{ke}\rho g \\ S'_{ske} &= \alpha'_{ke}\rho g \end{aligned}\right\} \; for\ \sigma_e \leq \sigma_{e(max)}$$

$$\left.\begin{aligned} S_{skv} &= \alpha_{ke}\rho g = 0 \\ S'_{skv} &= \alpha'_{ke}\rho g \end{aligned}\right\} \; for\ \sigma_e > \sigma_{e(max)}$$

where the subscripts e and v stand for elastic and inelastic, respectively, and primes represent aquitards. Generally, the inelastic compressibility of aquifers is small enough to be considered negligible. The product of the skeletal specific storage (S_{sk}) and the height of the corresponding aquifer-system unit equals the storage coefficient (S) of that particular unit:

$$S = S_{sk}b$$

The specific storage of water (S_{sw}) can also be determined by the product of water compressibility (β_w), density of water (ρ), and gravitational acceleration (g):

$$S_{sw} = \beta_w\rho g$$

The specific storage of water (S_{sw}) is considered negligible for aquifer-systems within the inelastic range of stress but within the elastic range of stress it may be a significant component. The specific storage of water (S_{sw}) refers to the volume of groundwater stored due to the compressibility of water (Freeze and Cherry, 1979). The aquifer-system specific storage can be calculated by summing each calculated skeletal specific storage and the specific storage of water. Matrix compressibility is typically several orders of magnitude greater than water compressibility, especially for the sediments present at the Lorenzi site, therefore the contribution from water expansion is considered negligible (Burbey, 2003).

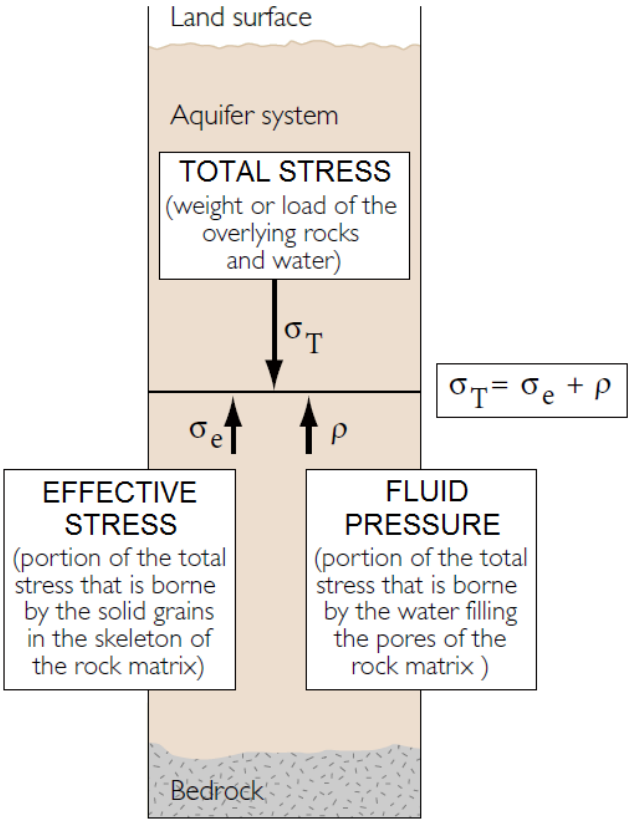

Figure 8: Terzaghi's principle of effective stress states at any point in an aquifer-system fluid pressure and effective stress supports the total stress acting upon it (1925, 1943) (modified from USGS, 1999).

1.4.3 Theory of Hydrodynamic Consolidation

The theory of hydrodynamic consolidation (Terzaghi, 1925, 1943) explains the relationship between declining head levels in adjacent aquifers to an aquitard's delayed equilibration and residual compaction (Figure 7). Aquitards are slow to reach equilibration with adjacent pumped aquifers because of the delayed aquitard head change. When water is pumped from an aquifer, resulting in a change in aquifer head, the adjacent aquitard head change lags behind because aquitards have a much smaller permeability which causes a slower rate of drainage. Typically, thick aquitards that experience seasonal pumping do not have enough time for fluid pressures to equilibrate before a new pumping cycle begins. If the aquitard internal effective stress exceeds the preconsolidation stress ($\sigma_{e(\max)}$) inelastic compaction occurs.

Aquitard inelastic compaction resulting from an effective stress (σ_e) greater than the preconsolidation stress ($\sigma_{e(\max)}$), which has not yet occurred because of delayed equilibration of aquitard heads relative to the adjacent aquifers, is known as residual compaction (Poland et al., 1972). Riley (1969) introduced the concept of an aquitard time constant, which describes how long it would take for the aquitard to compress to 93 percent of its total compaction, corresponding to a particular head decline, for a doubly draining aquitard. A doubly draining aquitard releases water to both the overlying and underlying adjacent aquifers, which are assumed to have identical lowered head changes. Aquitard inelastic skeletal specific storage (S'_{skv}), aquitard thickness (b'), and aquitard vertical hydraulic conductivity (K'_v) express the time constant (τ) as follows:

$$\tau = \frac{S'_{skv}(\frac{b'}{2})^2}{K'_v}$$

Epstein (1987) determined a time constant could be estimated for an aquitard with only one adjacent aquifer by replacing the ($\frac{b'}{2}$) with b'.

CHAPTER 2: METHODS

2.1 DATA COLLECTION

The 1994-2007 groundwater level record collected at the Lorenzi site was obtained from the Groundwater for USA: Water Levels data base (USGS, 2016). Water-levels for the three wells can be accessed by searching each well's site number, listed in Appendix A. The extensometer site number is also listed however to obtain the data record from the extensometer an email must be sent to the Nevada Water Science Center Water-Data Inquiries as the record is maintained by the USGS Nevada Water Science Center.

2.2 SIGNAL PROCESSING

Three distinct temporal scales of water-level changes can be observed in the water-level record from the Lorenzi site. Due to the scale of the graph only two of the water-level signals are shown in Figure 9. The first signal is the daily signal, comprised of hourly depth to water-level values for the three vertically separated confined aquifers. Large daily water-level fluctuations for both the middle and deep aquifers were the result of diurnal pumping, where the production wells were shut off during the day but pumped during the night and morning. As can be seen in Figure 9, the shallow aquifer daily head changes were extremely small compared to the middle and deep aquifers, around 0.03 m, therefore graphically the daily signal was not observed in the shallow aquifer.

The second signal is the seasonal signal, which reflected the seasonal increased pumping volume during the summer months, from May through September, and reduced pumping during winter, October through April. In Figure 9, the seasonal signal can be seen in the water-record for all three aquifers, creating the overall wavy appearance of the three lines. The seasonal signal can also be seen in Figure 10 causing the stair-step appearance of the long-term compaction record.

The final signal is the decadal signal, which was the long-term trend in compaction occurring at the Lorenzi site. The overall downward sloping trend in Figure 10 is the long-term compaction trend while the stair-step pattern is the seasonal signal superimposed on the decadal signal. The long-term compaction trend was the result of water-level declines that exceeded the past maximum effective stress of the aquifer-system from many decades of previous groundwater drawdown. As water-levels began to increase, starting in 1999, the rate of decadal compaction started to decline as a result of a lessening difference in head between the aquitards

and aquifers. Since the compacting aquitards drain much more slowly than the aquifers the seasonal pumping does not appear to affect the long-term compaction trend. All three signals are rather superimposed on one another producing the overall total data record.

A smoothing process and signal filter were used to extract the seasonal and decadal signals from the subsidence and water-level daily data records. The low-pass filter was developed, and described in detail, by Godin (1972). In summary an average value was assigned to the center of n consecutive data points that were averaged. The n data points were represented by A_n, the average of the n data points was represented by $\frac{A_n}{n}$ and both signal filters had the form $\frac{A_n 2\ A_n+1}{n^2(n+1)}$ which used three averaging operations. A FORTRAN program (Lahey Computer Systems, Inc., 2002) was written to perform the smoothing process and low-pass filter and can be found in Appendix B.

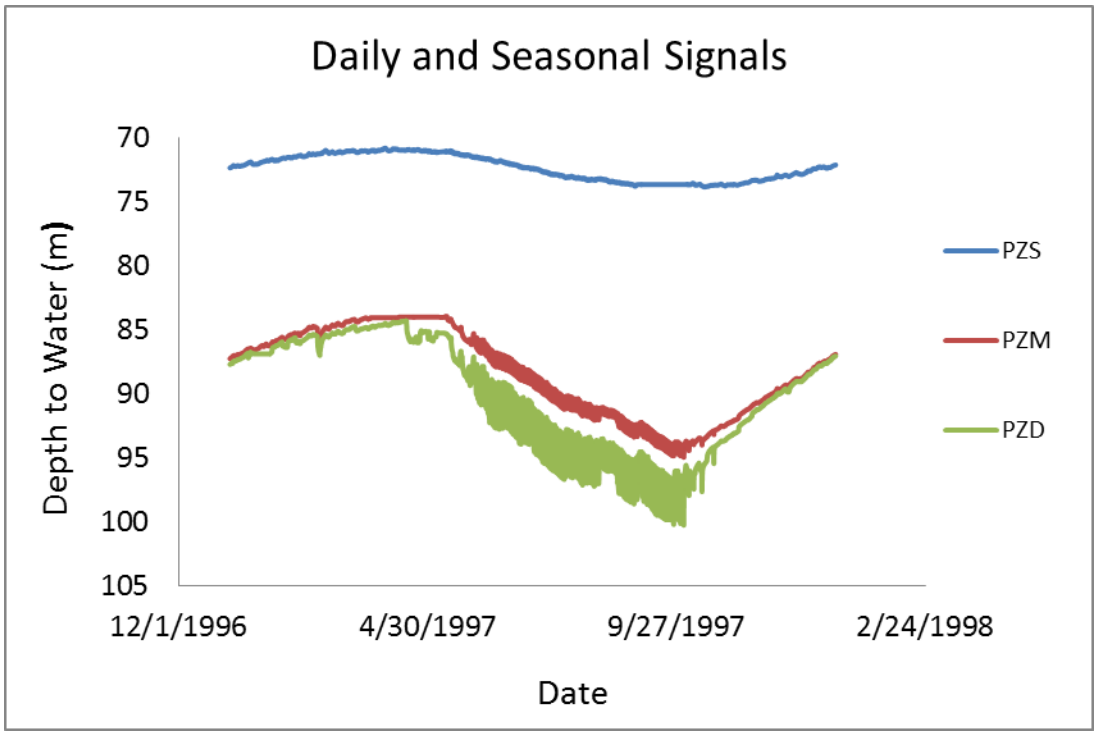

Figure 9: Depth to water-level for the three nested aquifers (PZS = shallow, PZM = middle, and PZD = deep aquifer) from January 1st, 1997 to January 1st, 1998 showing the daily and seasonal signals. The daily signal is observed as 'noise' in the middle and deep aquifers. The seasonal signal created the overall wavy appearance in the lines.

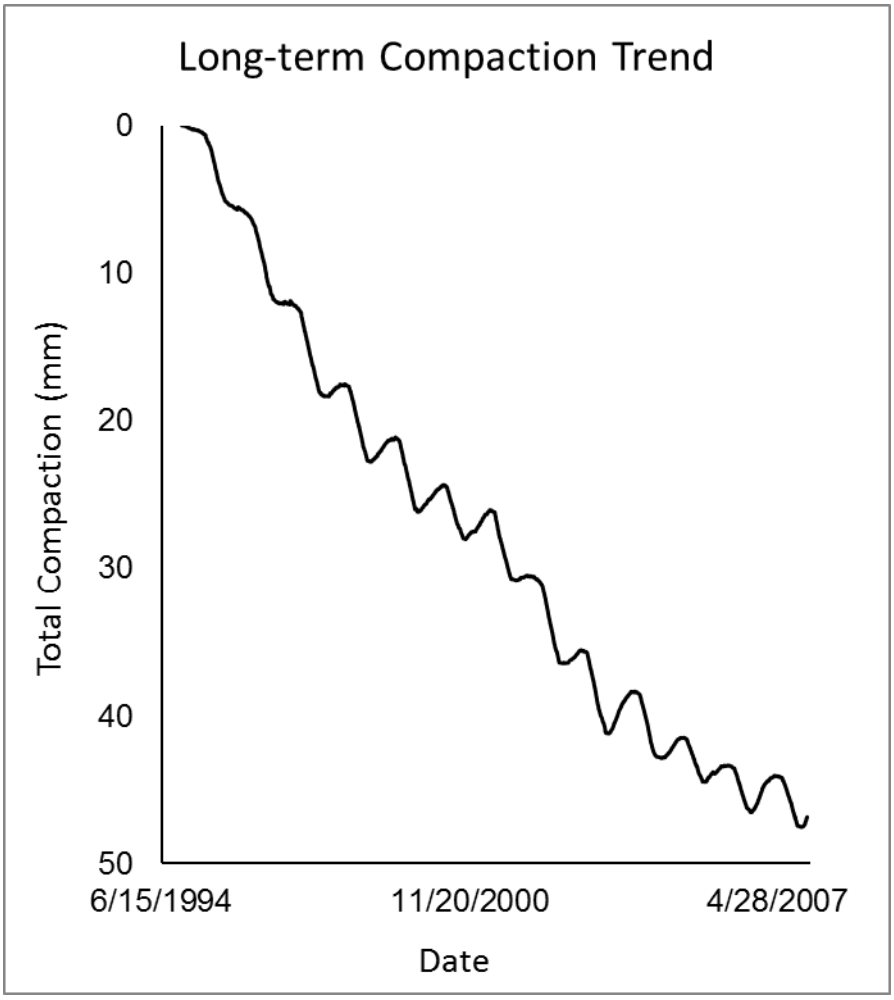

Figure 10: Total compaction record of the aquifer-system at the Lorenzi site showing the long-term compaction trend. The stair-step appearance was the result of the seasonal signal.

2.3 DAILY SIGNAL

2.3.1 AquiferTest Pro

The diurnal pumping that occurred at the Lorenzi site was thought of as daily pumping tests, which are one of the most fundamental ways by which aquifer parameters are determined. Leaky single-layered aquifer methods are well-known techniques used by groundwater practitioners with pumping test data to quantitatively estimate aquifer transmissivity and storage

coefficient values (Kruseman and Ridder, 1994). Multi-layered aquifer-systems, such as the Lorenzi site aquifer-system, are considered 'leaky' when groundwater flows through confining layers to an adjacent pumped aquifer at large enough volumes to be detected when observing drawdown in the pumped aquifer (Neuman and Witherspoon, 1969). The software package AquiferTest Pro (Waterloo Hydrogeology Inc., 2014) was used to calculate the aquifer parameters by performing the leaky single-layered aquifer methods.

The confined middle and deep aquifers, along with the deep aquitard (Figure 6), were considered their own multi-layered aquifer-system. The shallow aquifer was not included because the daily head change experienced in the shallow aquifer was less than 1% of the total head change experienced in all three of the aquifers. Therefore, any pumping that occurred within the shallow aquifer was considered negligible. Since the shallow aquifer was not included, the upper aquitards were not required. The percent of head change that occurred in each aquifer is listed in Appendix C.

Hantush-Jacob's (Walton) method and Hantush's curve-fitting method, which takes into account the storage changes of the aquitards, were both utilized since the pumping time for each daily test was small enough that the drawdown in the unpumped layers could be assumed negligible (Kruseman and Ridder, 1994). Both methods were performed separately to act as a check on the estimated aquifer parameters and create a small range of reasonable values. Each method assumed an aquifer-system of infinite extent consisting of two homogeneous, isotropic leaky aquifers with uniform thickness separated by a homogeneous, isotropic aquitard with uniform thickness (Waterloo Hydrogeology Inc., 2014). The pumping well was assumed to be fully penetrating, pumped at a constant rate with a diameter small enough for wellbore storage to be assumed negligible, and have unsteady groundwater flow (Waterloo Hydrogeology Inc.,

2014). Also assumed is vertical flow in the aquitard, negligible drawdown in the unpumped aquifer, and that the lower aquifer was resting on an impermeable layer (Waterloo Hydrogeology Inc., 2014).

To estimate the aquifer transmissivity and storage coefficient values using the Hantush-Jacob (Walton) method, in AquiferTest Pro (Waterloo Hydrogeology Inc., 2014), the following solution was used:

$$s = \frac{Q}{4\pi T} W\left(u, \frac{r}{L}\right)$$

where

$$u = \frac{r^2 S_{ske}}{4Tt} \qquad and \qquad L = \sqrt{Tc}$$

and s is drawdown, T is aquifer transmissivity, Q is constant pumping rate, $W\left(u, \frac{r}{L}\right)$ is the Walton function, t is the elapsed time from the start of pumping, r is the distance between the pumping and observation wells, L is the leakage factor, and c is the hydraulic resistance. The hydraulic resistance, how slowly infiltration is due to leakage, was determined using the deep aquitard parameters and the following equation:

$$c = \frac{b'}{K_v'}$$

where b' is the thickness of the aquitard and K_v' is the vertical hydraulic conductivity of the aquitard (Waterloo Hydrogeology Inc., 2014).

The hydraulic resistance could be calculated since the deep aquitard's vertical hydraulic conductivity was estimated from the seasonal signal. A log/log plot of the Walton function, on the y-axis, and $\frac{1}{u}$, on the x-axis, was used as a type curve and automatically matched to the pumping test data, plotted as time along the x-axis and drawdown along the y-axis, by

AquiferTest Pro (Waterloo Hydrogeology Inc., 2014). Dividing the estimated transmissivity and storage coefficient by each aquifer's thickness determined the horizontal hydraulic conductivity and elastic skeletal specific storage, respectively, for the middle and deep aquifers.

The Hantush – Storage in Aquitard method was solved, in AquiferTest Pro (Waterloo Hydrogeology Inc., 2014), using the follow solution:

$$s = \frac{Q}{4\pi K_h b} W(u, \beta)$$

where

$$u = \frac{r^2 S_{ske}}{4 K_h b t} \qquad and \qquad \beta = \frac{r}{4}\sqrt{\frac{\frac{K_v'}{b'}}{K_h b} \times \frac{S_{ske}'}{S_{ske}}}$$

and K_h is the horizontal hydraulic conductivity of the aquifer, b is the aquifer thickness, $W(u, \beta)$ is the Hantush function, S_{ske} is the aquifer elastic skeletal specific storage, and S_{ske}' is the aquitard elastic skeletal specific storage. As before, a type curve was generated by AquiferTest Pro (Waterloo Hydrogeology Inc., 2014) and automatically matched to the pumping test data. To satisfy the assumption that the drawdown in the unpumped aquifer was negligible, the adequate period of time for the pumping test was determined by:

$$t < \frac{S' b'}{10 K_v'}$$

where S' is the aquitard storage coefficient (Waterloo Hydrogeology Inc., 2014).

However, before AquiferTest Pro (Waterloo Hydrogeology Inc., 2014) could be used the average constant pumping rate, $4258.1 \frac{m^3}{hr}$, had to be partitioned between the middle and deep aquifers. The average constant pumping rate was calculated using the total volume of water pumped from the LVVWD well field over a known period of time. The initial division of the

constant pumping rate was based on the middle and deep aquifer thicknesses, since the specific aquifers being pumped by each pumping well in the LVVWD well field was unknown. The initial proportioning was used as a base case from which 5 iterations were performed by increments of 5%. During each iteration the pumping rate of the middle aquifer increased by $213\ \frac{m^3}{hr}$ while the deep aquifer pumping rate decreased by the same amount. The final iteration resulted in an even division of the pumping rate between the middle and deep aquifers.

There is no subsidence record associated with the daily signal therefore it can be assumed that the elastic skeletal specific storage values estimated are a reflection of only the elastic component of the aquifers and the inelastic component can be ignored. The daily fluctuations observed in the subsidence record were determined to be the result of the heating and expansion of the above ground extensometer hardware during the day since no daily compaction fluctuations are observed during the cooler months when daily temperatures are not as extreme (Pavelko, 2000). Pavelko (2004) suggested the extensometer could not pick up the quick compaction fluctuation because of an accuracy and efficiency limitation, but the lack of a daily subsidence record could also just be the result of the compaction being too small for observation.

2.4 SEASONAL SIGNAL

2.4.1 Stress-Strain Plots

Stress-strain plots were used to estimate the average elastic skeletal specific storages for the three aquitards at the Lorenzi site. Riley (1969) demonstrated that estimated aquitard elastic and inelastic skeletal storage coefficients could be graphically calculated from stress-strain plots assuming a constant total stress was acting on the aquifer-system. The inverse slope of the change in measured compaction (strain) versus the measured head change (stress) equaled the estimated aquitard skeletal storage coefficient (Riley, 1969).

Stress-strain plots were created from each of the aquifer's seasonal changes in water-level records as well as the changes that occurred in total compaction record, which was partitioned based on the fraction of total head change for each particular aquifer. Since each aquifer's seasonal record contains twelve seasonal cycles (years) twelve stress-strain plots were created, one for each year, and an averaged elastic skeletal specific storage was determined for each aquifer. Dividing the elastic skeletal storage coefficients by the respective aquifer thickness resulted in an estimated elastic skeletal specific storage for each of the aquitards. The table showing the total compaction partitioning and the 36 stress-strain plots for the three aquifers can be found in Appendix D.

2.4.2 Maximum Cross-correlation and Time Constant Equation

To determine the average lag time between the seasonal subsidence and three aquifers' seasonal water-level records the time series analysis maximum cross-correlation (Figure 11) was performed in R (R Code Team, 2012), which revealed the maximum overall correlations between the water-levels and subsidence records. Maximum cross-correlation determines to what degree a signal must be shifted along the x-axis for a maximum alignment with a second signal to be reached (Figure 11) (Rhudy et al., 2009). The seasonal record was split into yearlong intervals, from 1995 to 2006, for which a maximum correlation was determined. The calculated maximum correlation related to the lag time, in days, between the seasonal subsidence and water-level data from each aquifer. The 12 lag times determined, for each aquifer, were then averaged. The R code used to perform the time series analysis is located in Appendix E.

The lag times and previously determined aquitard elastic skeletal specific storage values were used with the aquitard-drainage model time constant equation to calculate the vertical hydraulic conductivities for the middle and deep aquitards:

$$\tau = \frac{S'_{ske}(\frac{b'}{2})^2}{K'_v}$$

where S'_{ske} is the elastic skeletal specific storage, K'_v is the aquitard vertical hydraulic conductivity, τ is the time constant (lag time), and b' is the thickness of the doubly draining aquitard. Since the shallow aquitard was in contact with only one adjacent aquifer the time constant equation had to be modified to contain only b' instead of $\frac{b'}{2}$ (Epstein, 1987).

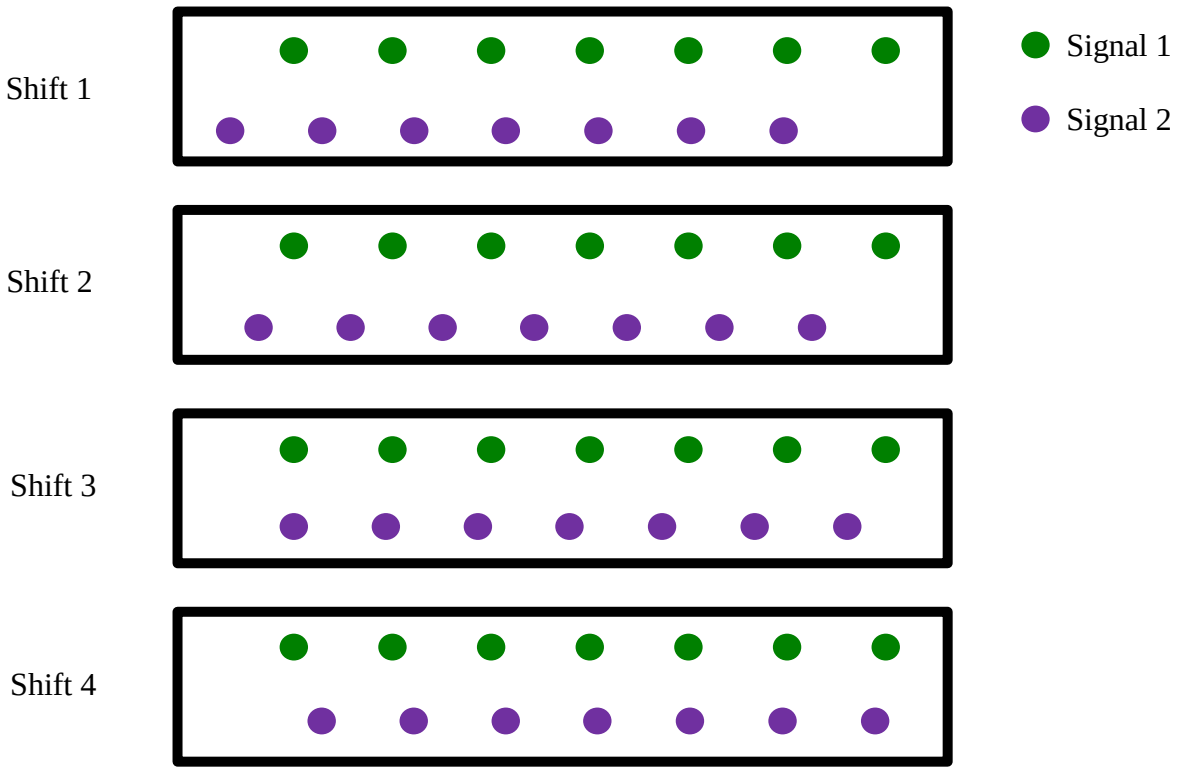

Figure 11: Example of maximum cross-correlation between two signals. The second signal will be shifted along the x-axis until a maximum alignment is reached between the two signals.

2.4.3 Hydraulic Diffusivity

Hydraulic diffusivity describes the ratio of hydraulic conductivity to specific skeletal storage. The aquitard-drainage model time constant equation was rearranged to determine the hydraulic diffusivity (D) for each of the three aquitards based on the estimated seasonal signal time lag (τ) and thicknesses of the adjacent aquitards (b'):

$$D = \frac{K'_v}{S'_{ske}} = \frac{(\frac{b'}{2})^2}{\tau}$$

Hydraulic diffusivity values were also determined using the estimated aquitard elastic skeletal specific storage (S'_{ske}) and vertical hydraulic conductivity (K'_v) values calculated from the seasonal signal data. As mentioned previously, the time constant equation had to be modified to contain b' instead of $\frac{b'}{2}$ for the shallow aquitard since it is adjacent to only one aquifer (Epstein, 1987).

2.5 DECADAL SIGNAL

2.5.1 Stress-Strain Plots

Stress-strain plots were also used to estimate an average inelastic skeletal specific storage for the aquitard unit at the Lorenzi site. As previously stated, by plotting total compaction (strain) versus depth to water-level (stress) Riley (1969) demonstrated that estimated aquitard inelastic skeletal specific storage could be graphically calculated, assuming a constant total stress was acting on the aquifer-system. The aquitard inelastic response plots as a dominant linear trend after the elastic response, hysteresis loops, on the stress-strain plots (Pope and Burbey, 2004). The inverse slope to this dominant linear trend equaled the estimated aquitard inelastic skeletal storage coefficient (Riley, 1969).

A stress-strain plot was created using depth to water-levels, averaged from the three aquifer average daily water-level records, along with average daily total compaction. Around 1999 the pumping rates greatly declined allowing the water-levels in each aquifer to rise which resulted a rate change in the long-term compaction at the Lorenzi site. Only the data record from 1994 to 2001 was used to create the decadal signal stress-strain plot to reduce the influence of the long-term compaction rate change. Suitable inelastic response trends, the near linear trends extending out after the presence of a hysteresis loop, were then located and inverse slopes were determined. The estimated inverse slopes were divided by the average thickness of all three aquifers to obtain the average inelastic skeletal specific storage for the aquitard unit.

2.6 PRINCIPAL COMPONENTS ANALYSIS

Principal Components Analysis (PCA) was used to statistically verify the presence of the three temporal signals within the total data record. PCA is a statistical procedure that estimates the principal components of a data set, which represent the underlying structure and best explains the variance within the data (Smith, 2002). Using R (R Code Team, 2012), PCA was performed on the complete average daily data record, where the three aquifers' water-levels and total subsidence record formed the column variables and each day of the data record were the row observations.

PCA was also performed on daily and monthly values for the shallow aquifer, middle aquifer, deep aquifer, and total subsidence records individually. The daily analysis had 12 months of the year as the rows and 28 days of each month as the column variables. The data input for the daily analysis were averaged daily values from 1995 to 2007. The monthly analysis had 13 years, from 1995 to 2007, form the rows and the 12 months of each year as the column

variables. The data input for the monthly analysis were averaged monthly values from 1995 to 2007.

Varimax and oblimin rotations were also conducted on the resulting principal components for each monthly analysis to simplify the results for easier interpretation. Two main types of rotations are used to simplify interpretations of PCA results; orthogonal, assumes variables in the analysis are uncorrelated, and oblique, assumes variables in the analysis are correlated (Abdi and Williams, 2010). The varimax rotation is a popular orthogonal rotation, which keeps the new axes of the rotated matrix orthogonal to each other, while the oblimin rotation is a form of oblique rotation, which does not require the new axes to be orthogonal (Abdi and Williams, 2010).

The varimax rotation was performed on all 12 principal components while the oblimin rotation was performed on only the first four principal components. For each analysis performed, the rows containing missing data were eliminated and the observations were centered by subtracting the average of each respective column from the column values. The R code for each analysis can be found in Appendix F along with diagrams showing the variables and observations for each.

CHAPTER 3: RESULTS

3.1 DAILY SIGNAL

3.1.1 AquiferTest Pro

The upper and lower limit estimations of horizontal hydraulic conductivity and elastic skeletal specific storage for the middle and deep aquifers are shown in Table 4. The aquifer parameters determined by the Hantush-Jacob (Walton) and Hantush – Storage in Aquitard methods in AquiferTest Pro (Waterloo Hydrogeology Inc., 2014) agree well, with a difference of

a factor of 6 between the horizontal hydraulic conductivity values for the middle aquifer and a factor of about 4 for the deep aquifer. The aquifer elastic skeletal specific storage values are also nearly identical between the two methods.

The table in Appendix G shows the middle and deep aquifer's estimated parameters for the base case, the pumping rate proportioned based on aquifer thicknesses, and each successive 5% iteration. The calculation for hydraulic resistance, used in the Hantush-Jacob (Walton) method, can also be found in Appendix G. The elapsed time that would be adequate for the use of the daily signal data with the Hantush – Storage in Aquitard method is calculated in Appendix Has well. Finally, the partitioned pumping rates based on the aquifer thicknesses are also in Appendix G.

The estimated deep aquifer parameters are expected to be somewhat smaller compared to the middle aquifer, due to the larger total stress borne by the deep aquifer. As discussed earlier, Terzaghi's principle of effective stress states that any point in an aquifer-system has a total stress acting upon it, which is supported by the fluid pressure and effective stress at that point (1925, 1943). Even before the effective stress of the deep aquifer was increased by pumping, the deep aquifer would have had a larger fluid pressure and effective stress since the total stress acting on the deep aquifer included the overlying weight of the rest of the aquifer-system at the Lorenzi site.

The composition of the middle and deep aquifers could play a role in the difference in estimated parameters as well. The aquifer-system present in Las Vegas Valley is dominated by sand and gravel near the margins of the valley but those layers become more discontinuous towards the eastern and central parts, due to the increase of clays and silts (Pavelko, 2004). This pattern resulted in the confined aquifers being composed of permeable sand and gravel layers

interspersed among clay and silt layers, which may have resulted in some interfingering clay and silt layers within the gravel and sand layers during deposition. The deep aquifer being 35 m thicker allows for a greater chance of thin discontinuous clay and silt layers to have been deposited during the sediment deposition of the gravel and sand, becoming a possible contributing factor to the difference in estimated aquifer parameters since clay and silt naturally have smaller elastic skeletal specific storage and hydraulic conductivity values compared to gravel and sand.

The calculated upper and lower elastic skeletal specific storage limits for the deep aquifer (Table 4) fall within the reasonable range of estimated values based on Hanson (1989) and reported in Pavelko (2004) (Table 5). The deep aquifer lower limit is nearly identical to Pavelko's (2004) optimal aquifer unit estimate (Table 5). The middle aquifer's lower elastic skeletal specific stoarge limit (Table 4) nearly over laps with the upper estimate of the reasonable range (Table 5) and is within the same magnitude. The middle aquifer's lower limit is also within the same magnitude as Pavelko's (2004) optimal aquifer unit estimate (Table 5). Hanson's (1989) elastic specific storage range was estimated using the numerical model COMPAC (Helm, 1974, 1975) to simulate vertical aquifer-system compaction in Aura Valley and Tucson Basin, Arizona. Pavelko's (2004) optimal estimate was obtained after evaluating the 1-dimensional numerical model on the Lorenzi site vertical aquifer-system compaction.

Table 4: Estimated upper and lower aquifer horizontal hydraulic conductivity and elastic skeletal specific storage limits determined using the Hantush-Jacob (Walton) and Hantush – Storage in Aquitard methods with the diurnal pumping data in AquiferTest Pro (Waterloo Hydrogeology Inc., 2014).

Aquifer		**Hantush-Jacob (Walton)**		**Hantush – Storage in Aquitard**	
		K_h	S_{ske}	K_h	S_{ske}
		m/day	1/m	m/day	1/m
Middle	Upper limit	323	1.2×10^{-5}	319	1.1×10^{-5}
	Lower limit	188	6.7×10^{-6}	184	6.6×10^{-6}
Deep	Upper limit	69	1.7×10^{-6}	66	1.6×10^{-6}
	Lower limit	48	1.2×10^{-6}	46	1.2×10^{-6}

Table 5: The reasonable range and optimal estimate for the Lorenzi site aquifer unit elastic skeletal specific storage. The reasonable range is based on estimated values determined using the numerical model COMPAC (Helm, 1974, 1975) by Hanson (1989) and an optimal estimate evaluated by Pavelko (2004) using a 1-dimensional numerical model of the Lorenzi site aquifer-system.

		S_{ske}
		1/m
Reasonable range	Upper estimate	7×10^{-6}
	Lower estimate	1×10^{-7}
Pavelko's optimal estimate		1×10^{-6}

3.2 SEASONAL SIGNAL

3.2.1 Stress-Strain Plots

Figure 12 shows the calculated average elastic specific storage values for the three vertically separated aquitards at the Lorenzi site. A relationship between the three aquitards show the elastic specific storage value becoming increasingly smaller as the depth below land surface increases. Inversely, the greater the depth below land surface the greater the margin of error, with the largest being $2.02^{-6}\ \frac{1}{m}$ for the deep aquitard. The table containing each aquitard's 12 individual seasonal cycles elastic specific storage values as well as the subsequent averaged values, standard deviations, and margin of errors can be found in Appendix H. The calculated average aquitard elastic specific storage values (Figure 12) fall within the reasonable range of estimated values, again based on Hanson (1989) and reported in Pavelko (2004) (Table 6), and are only about one order of magnitude smaller than Pavelko's (2004) optimal aquitard unit estimate (Table 6).

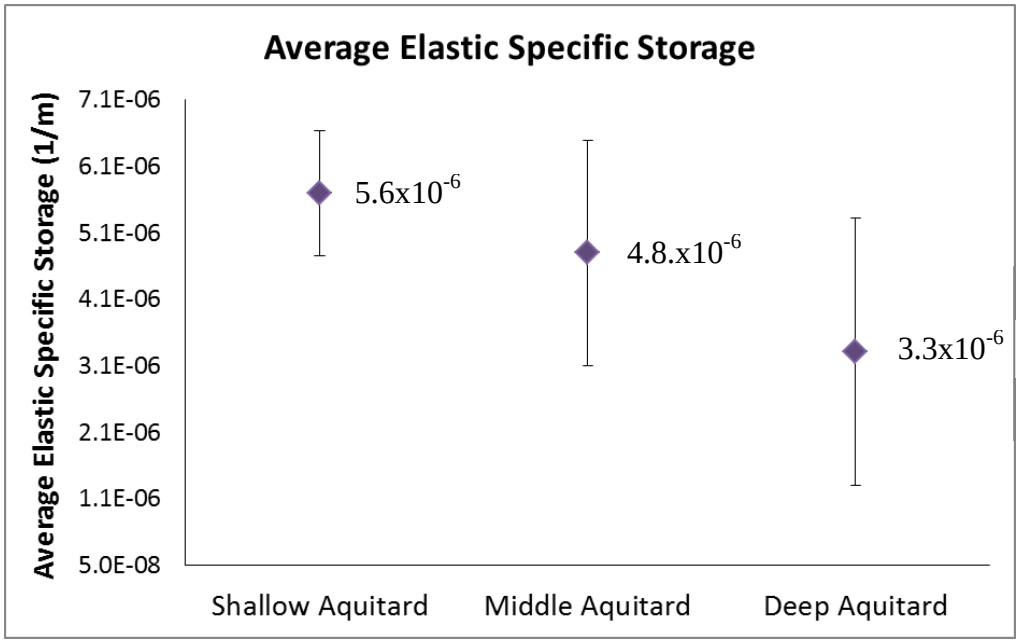

Figure 12: Average elastic skeletal specific storage calculated from the seasonal signal stress-strain plots for each of the three vertically separated aquitards at the Lorenzi site.

Table 6: The elastic skeletal specific storage reasonable range and optimal estimate for the Lorenzi site aquitard unit. The reasonable range is based on estimated values determined using the numerical model COMPAC (Helm, 1974, 1975) by Hanson (1989) and an optimal estimate evaluated by Pavelko (2004) using a 1-dimensional numerical model of the Lorenzi site aquifer-system.

		S'_{ske}
		1/m
Reasonable range	Upper estimate	$7x10^{-5}$
	Lower estimate	$3x10^{-6}$
Pavelko's optimal estimate		$2x10^{-5}$

3.2.2 Maximum Cross-correlation and Time Constant Equation

Average hydrodynamic lag times for the three vertically separated aquitards at the Lorenzi site are show in Figure 13. The lag times, in days, increase as the aquitards increase in depth below land surface. The margin of error across all three aquitards stays constant at about 4 days. The table showing each aquitard's 12 individual yearlong maximum correlation lag times and subsequent averaged values, standard deviations, and margin of errors can be found in Appendix I.

The trend of lag times increasing as each aquitard's depth increases below land surface may be explained by the amount of head change that occurs in each aquifer. The shallow aquifer experiences the smallest changes in head over a seasonal cycle while the deep aquifer experiences the largest. The deep aquitard is positioned between both the middle and deep aquifers, which experiences larger changes in head and which requires a longer time to equilibrate. The shallow aquitard is adjacent only to the shallow aquifer so the head changes required to equilibrate to are much smaller, which causes the shallow aquitard to have a much smaller lag time compared to the other two aquitards.

The hydrodynamic lag times describe the number of days it takes for the elastic change in compaction of each aquitard to reflect the elastic change in head of each aquifer. Changes in aquitard compaction result when aquitard head levels equilibrate with the adjacent fluctuating aquifer head levels. Compared to aquifers, aquitards experience a natural delayed change in head due to an aquitard's reduced permeability (Freeze and Cherry, 1979). The seasonal pumping implemented by the LVVWD allows only a fraction of the groundwater stored in the aquitards to be released to the aquifer-system before the pumping is ceased and the aquifer and aquitard head

levels are able to recover. The seasonal pumping allows some aquitard stored groundwater to be available for pumping while not causing any permanent land subsidence.

Table 7 displays the estimated vertical hydraulic conductivities for the three aquitards at the Lorenzi site. Upper and lower limits of the vertical hydraulic conductivities are shown based on the margin of error of the previously calculated aquitard elastic specific storage values (Figure 12). The estimate decreases as the depth below land surface increases for each successive aquitard.

This observed trend is most likely the result of the aquitards' soil matrix properties, which include; porosity as well as pore size distribution, pore shape, and granular alignment – all factors that control permeability (Delage and Lefebvre, 1984). Porosity describes the volume or pore spaces within a sediment while permeability describes how well interconnected those pore spaces are (Freeze and Cherry, 1979). Permeability is directly related to hydraulic conductivity (Rudolph and Frind, 1991):

$$K = \frac{k\rho g}{\mu}$$

where K is hydraulic conductivity, k is permeability, ρ is fluid mass density, g is gravitational acceleration, and μ is fluid viscosity.

Two processes could explain why the three aquitards could have differing hydraulic conductivity. Firstly, the porosity and permeability of a sediment can be reduced by the weight of overlying materials causing sediments located deeper below land surface to have smaller porosities and permeabilities compared with identical sediments at land surface (Whipkey and Kirkby, 1987). This is especially true for clay and silt grains, which compose most aquitards, since they have a platy flat structure allowing the grains to realign to a more compressed form

perpendicular to an applied stress or pressure, such as the deposition of overlying sediment (Freeland, 2013).

The rearrangement of an aquitard's grain matrix, due to surpassed preconsolidation stresses, can also lead to decreased porosity and permeability, again, due to the realignment of the matrix grains resulting in sediment compaction (Delage and Lefebvre, 1984). If the proportion of past compaction at the Lorenzi site was largest for the deep aquitard, and decreased as the depth below land surface decreased, the compaction that previously occurred could be the cause of the vertical hydraulic conductivity trend observed in the three aquitards. Realistically, some combination of these two processes likely created the observed trend.

The estimated aquitard vertical hydraulic conductivity values for the middle and deep aquitards (Table 7) also fall within the range of reasonable values reported by Pavelko (2004) while the shallow aquitard's value is within the same magnitude as the upper reasonable value (Table 8). This range of reasonable values was based on the estimations of aquitard vertical hydraulic conductivity from a number of studies done at sites in Las Vegas (Waichler and Cochran, 1991), Las Vegas Valley (Harrill, 1976), and central California (Riley, 1969; Sneed and Galloway, 2000). Compared to Pavelko's (2004) optimal aquitard unit estimate (Table 7) each of the estimated seasonal signal aquitard vertical hydraulic conductivity values (Table 6) are little more than an order of magnitude larger.

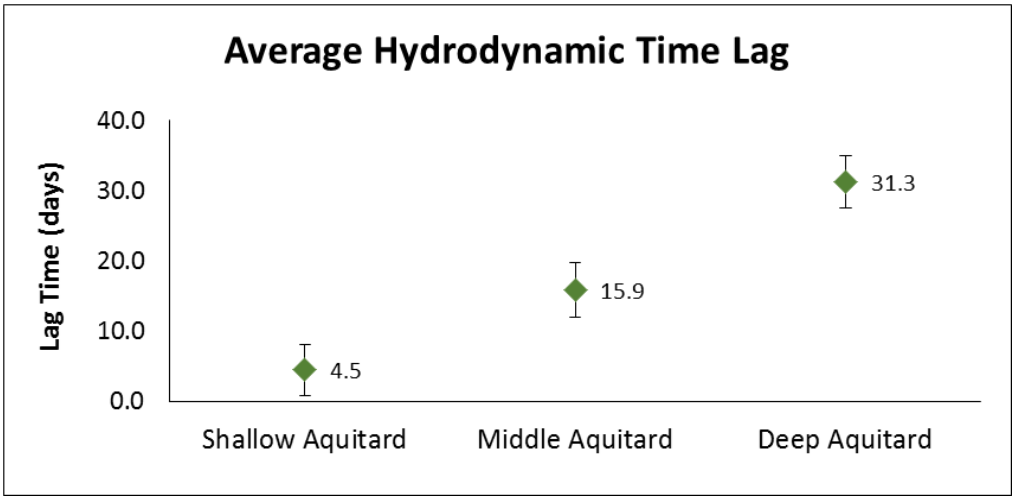

Figure 13: Average aquitard hydrodynamic lag times calculated from the maximum correlation between the seasonal signal change in water-level and change in compaction data for each of the three vertically separated aquitards at the Lorenzi site.

Table 7: Estimated aquitard vertical hydraulic conductivity calculated using the aquitard-drainage time constant equation, with upper and lower limits calculated based on the aquitard elastic specific storage margin of error, for each of the three vertically separated aquitards at the Lorenzi site.

Aquitard		b'	S'_{ske}	**Lag Time**	K'_v
		m	m^{-1}	days	m/day
Shallow	Upper limit	77.7	$6.6x10^{-6}$	4.5	$8.8x10^{-3}$
	Optimal estimate		$5.6x10^{-6}$		$7.6x10^{-3}$
	Lower limit		$4.7x10^{-6}$		$6.3x10^{-3}$
Middle	Upper limit	34.1	$6.4x10^{-6}$	15.9	$1.2x10^{-4}$
	Optimal estimate		$4.8x10^{-6}$		$8.7x10^{-5}$
	Lower limit		$3.0x10^{-6}$		$5.6x10^{-5}$
Deep	Upper limit	32.0	$5.3x10^{-6}$	31.3	$4.3x10^{-5}$
	Optimal estimate		$3.3x10^{-6}$		$2.7x10^{-5}$
	Lower limit		$1.2x10^{-6}$		$1.0x10^{-5}$

Table 8: The reasonable range and optimal estimate for the Lorenzi site aquitard unit vertical hydraulic conductivity. The reasonable range was determined from previous studies around the Lorenzi Site (Harrill, 1976), Las Vegas (Waichler and Cochran, 1991), and central California (Riley, 1969; Sneed and Galloway, 2000) and the optimal estimate was evaluated by Pavelko (2004) using a 1-dimensional numerical model of the Lorenzi site aquifer-system.

		K'_v
		m/day
Reasonable range	Upper estimate	$2x10^{-3}$
	Lower estimate	$6x10^{-7}$
Pavelko's optimal estimate		$9x10^{-7}$

3.2.3 Hydraulic Diffusivity

Table 9 shows the estimated hydraulic diffusivity values for the three aquitards at the Lorenzi site, calculated first by the rearrangement of the aquitard-drainage time constant equation utilizing the estimated aquitard lag times and thicknesses and then by the previously estimated seasonal signal aquitard vertical hydraulic conductivity (Table 7) and elastic specific storage (Figure 12) values. The hydraulic diffusivity values are all near identical matches for each aquitard. The large hydraulic diffusivity values obtained for the shallow aquifer appear to be the result of the combination of 1) the time constant equation modification required for aquitards adjacent to only one aquifer, 2) the shallow aquitard having the greatest aquitard thickness, and 3) the shallow aquitard having an extremely short lag time compared to the middle and deep aquitards.

Table 9: Estimated aquitard hydraulic diffusivity values calculated by rearranging the aquitard-drainage model time constant equation and by direct use of calculated aquitard vertical hydraulic conductivity and elastic specific storage determined from the seasonal signal.

Aquitard	Rearranged time-constant equation			Estimated values from seasonal signal		
	Lag Time	b'	D	S'_{ske}	K'_v	D
	days	m	m^2/day	m^{-1}	m/day	m^2/day
Shallow	4.5	77.7	1341.6	$5.6x10^{-6}$	$7.8x10^{-3}$	1342.2
Middle	15.9	34.1	18.3	$4.8x10^{-6}$	$8.7x10^{-5}$	18.3
Deep	31.3	32.0	8.2	$3.3x10^{-6}$	$2.7x10^{-5}$	8.2

3.3 DECADAL SIGNAL

3.3.1 Stress-Strain Plots

Figure 14 shows the decadal stress-strain plot and three suitable inelastic response trends whose slopes are used to estimate the average inelastic skeletal specific storage for the Lorenzi site aquitard unit. The slight change in slope observed in the three inelastic response trends is likely due to the increasing water-levels that began around the end of 1999, leading to the lowering of the effective stress below the preconsolidation stress rate change of the compaction at the Lorenzi site. The estimated average inelastic skeletal specific storage for the aquitard unit is shown in Table 10, along with the calculated slopes of the inelastic response trends taken from the decadal stress-strain plot. The calculated average aquitard unit inelastic skeletal specific storage (Table 10) falls within the range of reasonable values based on the estimations of aquitard unit inelastic specific storage from a number of studies done at sites in Las Vegas

Valley (Harrill, 1976; Morgan and Dettinger, 1996), central California (Sneed and Galloway, 2000), and Arizona (Hanson, 1989) (Table 11).

Although the average inelastic skeletal specific storage for the aquitard unit (Table 10) is one order of magnitude smaller than Pavelko's (2004) optimal estimate (Table 11), the calculated average correlates well with the previously estimated aquitard elastic skeletal specific storage values for the three aquitards at the Lorenzi site (Figure 12). The calculated average elastic skeletal specific storage for all three aquitards (Figure 12) are all also one order of magnitude smaller than Pavelko's (2004) optimal aquitard unit elastic skeletal specific storage. Generally, the inelastic skeletal specific storage of an aquitard is 1 to 3 orders of magnitude larger than the elastic skeletal specific storage of the aquitard (Pavelko, 2004).

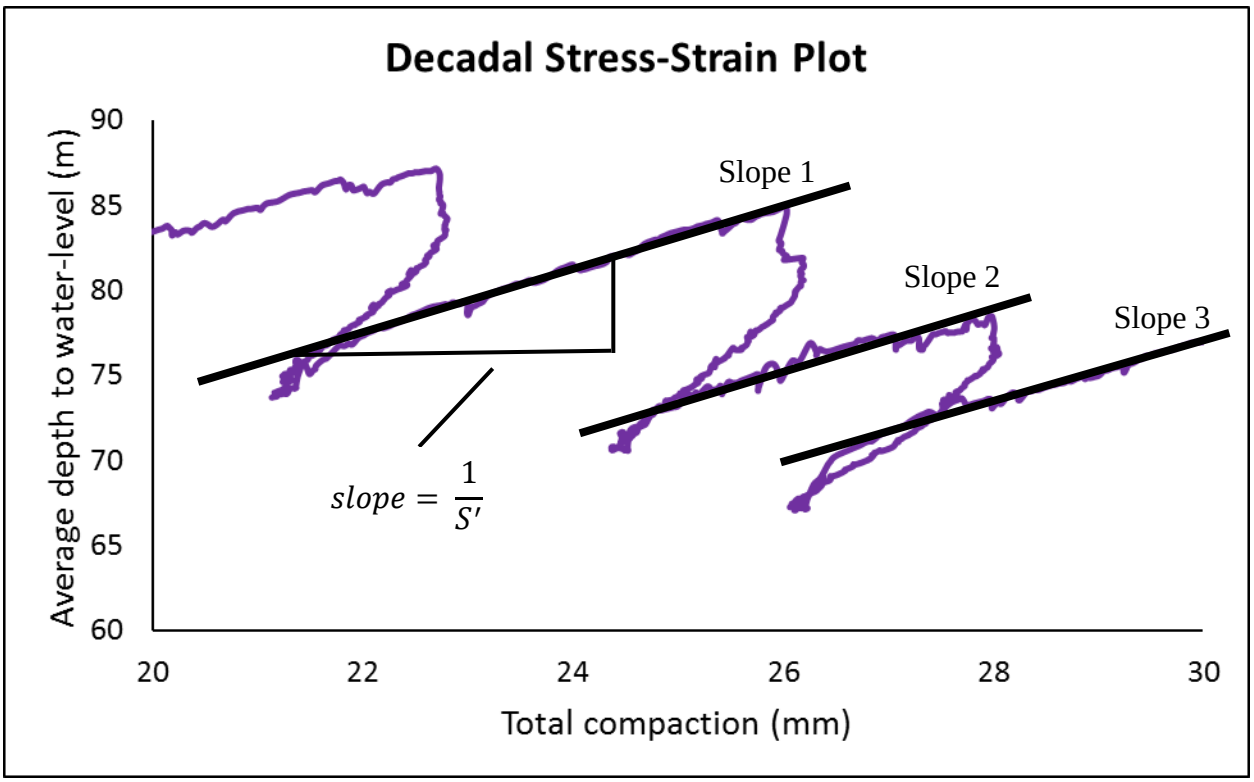

Figure 14: The three slopes of the suitable inelastic response trends from which an average inelastic skeletal specific storage was estimated for the Lorenzi site aquitard unit. The three slopes are determined from the stress-strain plot of depth to water-level, averaged from each aquifer daily average record, versus total average daily compaction. The inverse slope of the inelastic response trends equals the aquitard unit inelastic storage coefficient.

Table 10: Average inelastic skeletal specific storage for the Lorenzi site aquitard unit calculated from the inverse slope of the inelastic response trends from the decadal stress-strain plot divided by the average thickness of the three vertically separated confined aquifers.

		X-axis	Y-axis	Slope	Average b	S'_{skv}
		m	m		m	1/m
Slope 1	Point 1	0.0220	77	2083.3	36.3	$1.3x10^{-5}$
	Point 2	0.0244	82			
Slope 2	Point 1	0.0216	67	1875.0		$1.5x10^{-5}$
	Point 2	0.0248	73			
Slope 3	Point 1	0.0244	68	1590.9		$1.7x10^{-5}$
	Point 2	0.0288	75			
Average						$1.5x10^{-5}$

Table 11: The reasonable range and optimal estimate for the Lorenzi site aquitard unit inelastic skeletal specific storage. The reasonable range was determined from previous studies in Las Vegas Valley (Harrill, 1976; Morgan and Dettinger, 1996), central California (Sneed and Galloway, 2000), and Arizona (Hanson. 1989) and the optimal estimate was evaluated by Pavelko (2004) using a 1-dimensional numerical model of the Lorenzi site aquifer-system.

		S'_{skv}
		1/m
Reasonable range	Upper estimate	$3x10^{-3}$
	Lower estimate	$2x10^{-5}$
Pavelko's optimal estimate		$1x10^{-4}$

3.4 PRINCIPAL COMPONENTS ANALYSIS

Table 12 shows the results of the principal components analysis (PCA) on the complete average daily record. Principal component 1 (PC1) explains 89.6% of the variance in the data and the component loadings show an inverse relationship between the depth to water-levels for each aquifer (PZS, PZM, and PZD) and total subsidence (EXT1). PC1 is the only significant principal component having a variance equal to roughly 90%.

Table 12: Results from principal components analysis on the complete average daily record with variables of depth to water-levels for the shallow (PZS), middle (PZM), and deep (PZD) aquifers and total subsidence (EXT1).

Complete Average Daily Record	**PC1**	**PC2**	**PC3**	**PC4**
PZS	-0.507	-0.268	0.797	-0.190
PZM	-0.522	-0.214	-0.213	0.798
PZD	-0.512	-0.310	-0.565	-0.568
EXT1	0.478	-0.887	0.008	0.063
Importance of components				
Standard deviation	1.894	0.562	0.298	0.096
Proportion of Variance	0.896	0.079	0.023	0.002
Cumulative Proportion	0.896	0.975	0.998	1.00

The results for the PCAs on the daily and monthly values, as well as the rotated monthly principal components, are located in Appendix J. For brevity only the deep aquifer results are recorded and only the first six principal components of each analysis are listed. The similarities within each set of analysis results, each set includes the analysis of the shallow, middle, and deep

aquifers as well as the total subsidence records individually, allows the deep aquifer results to be a reasonable representation.

Over 99% of the variance in the data is explained by PC1 for each of the daily PCAs. PC1 is therefore the only significant principal component for each of the daily PCAs. Each analysis' component loadings for PC1 range within -0.180 and -0.191 and show no significant relationship between the 28-day variables. In addition, none of the variables show any strong relationship with PC1.

For each of the monthly PCAs over 90% of the variance in the data is explained by PC1. PC1 is again the only significant principal component for each of the monthly PCAs. Each analysis' component loadings for PC1 range within -0.23 and -0.32 and again no significant relationship is shown between the 12-month variables. No strong relationship between any of the variables and PC1 exists as well.

The varimax rotations, conducted on the 12 principal components obtained from each monthly PCA, show each of the 12-month variables equally explaining the variance in the data. Each 12-month variable having a component loading of 0.083. The oblimin rotations, conducted on the first four principal components obtained from each monthly PCA, show 99% of the variance explained by the first three principal components and a narrow range of component loadings for the each. However, the difference between the component loadings within each principal component is too small to show any significant relationship between the variables and the principal components.

The component loadings are listed as both standardized and unstandardized for the oblimin rotation results, but both sets show no significant relationship. The strength of the unstandardized component loadings for the first three principal components is shown in Figure

15, with plots of the depth to water-level for each month, averaged from 1995 to 2007, and the component loadings, multiplied by a scaler, of the first three principal components added and subtracted to the average monthly depth to water-level. Significant relationships are not observed in any of the plots.

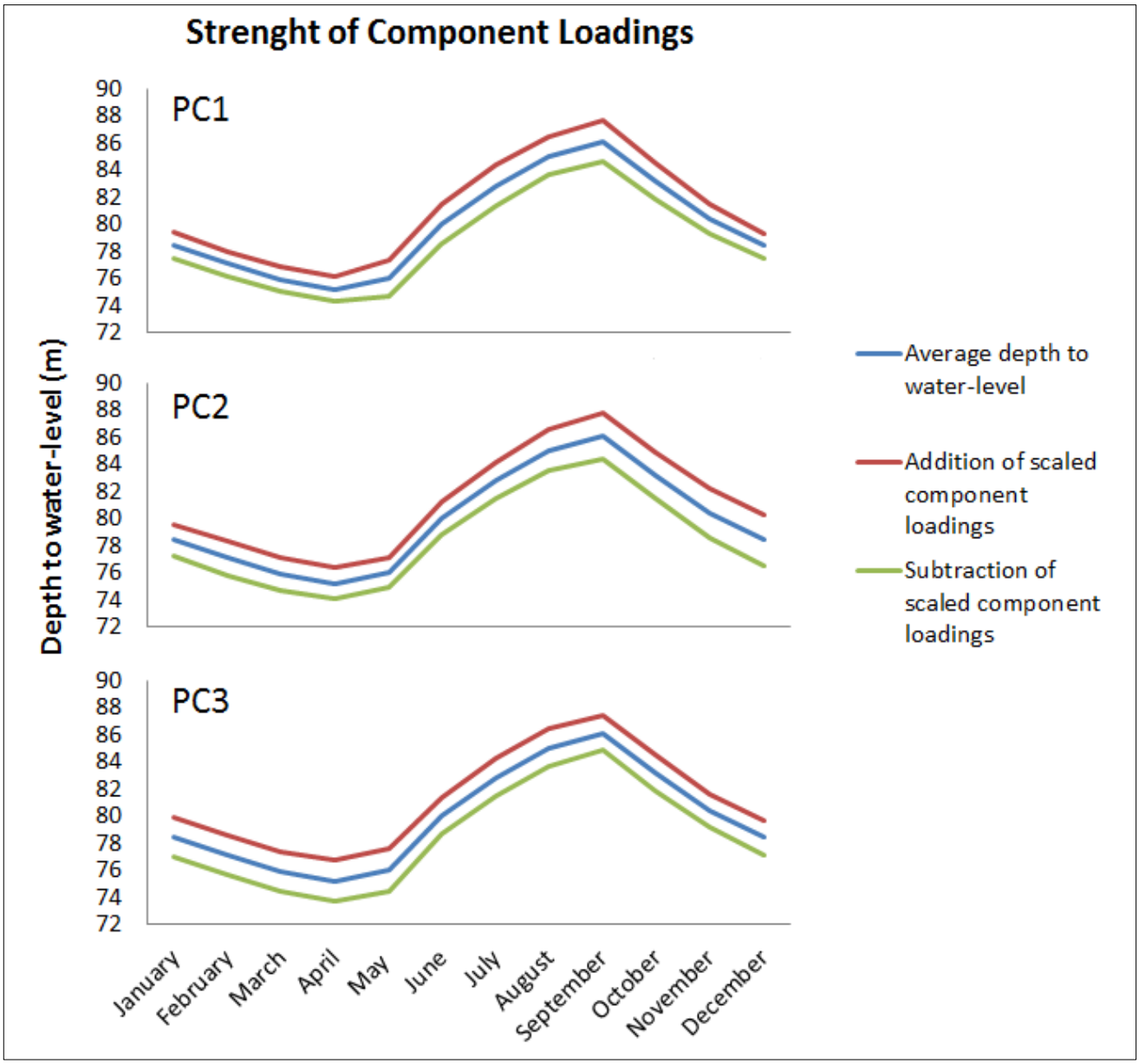

Figure 15: Strength of unstandardized component loadings for the first three principal components of the oblimin rotation, completed on the deep aquifer monthly PCA results, shown by adding and subtracting the scaled component loadings to the depth to water-level for each month, averaged from 1995 – 2007. No significant relationship is observed.

CHAPTER 4: DISCUSSION

Signal processing has been in the literature for a long time and through numerous studies been proven to be a versatile and effective tool for analyses. The elimination of short-term and long-term trends in water-level and compaction data is not a new form of analysis but been used in numerous other studies (Sneed and Galloway, 2000; Pope and Burbey, 2004). The method is also suitable for more than just subsidence studies having evolved from the study of earth tide effects on aquifer water-levels, which uses low-pass filters like the one developed by Godin (1972) to eliminate low-frequency data signals. One such example is the study by Hsieh et al. (1987) that used Godin's (1972) low-pass filter to determine aquifer transmissivity from analyzing earth tide interaction with the aquifer. Signal processing techniques can isolate otherwise obscured signals in data records which can be analyzed to gain a better understanding of the physical world from which the signals came.

4.1 DAILY SIGNAL

The diurnal water-level signal observed at the Lorenzi site is the result of diurnal pumping (pumping during the day and recovery during the night) at the LVVWD well field. This diurnal signal was evaluated using pumping test analyses, which allows for the estimation of the middle and deep aquifer parameters. Pumping tests are one of the most fundamental ways by which aquifer parameters are determined and can be utilized for a number of different aquifer-system arrangements. Theis and Cooper-Jacob methods were insufficient for the Lorenzi site aquifer-system which was determined to be leaky.

Some liberties had to be taken in order to determine a method that could use the daily signal data record to solve for those parameters. Only half of the aquifer-system was utilized with the Hantush-Jacob (Walton) and Hantush – Storage in Aquitard methods. A range of

partitioned pumping rates for the middle and deep aquifers was also determined based on the best-guessed practices of the LVVWD since the specific aquifers being pumped by each pumping well in the LVVWD well field was also unknown.

Although there were some assumptions made the resulting aquifer elastic skeletal specific storage estimates (Table 4) correlate well with the reasonable range of estimates reported in Pavelko (2004) (Table 5). The lower middle and deep aquifer estimates (Table 4) are even within the same magnitude as Pavelko's (2004) optimal estimate (Table 5). This agreement lends some credibility to the estimated horizontal hydraulic conductivity values (Table 4) as being reasonable estimates as well. The estimated aquifer parameters are also comparable to values determined for similar layered alluvial deposit aquifer-systems (Sneed and Galloway, 2000).

4.2 SEASONAL SIGNAL

Hydrodynamic lag is controlled by an aquitard's elastic specific storage and vertical hydraulic conductivity (Helm, 1984). Therefore, the estimated aquitard elastic skeletal specific storage values should correlate directly to the hydrodynamic lag times observed in the seasonal signal. To check this correlation hydraulic diffusivity values were calculated by first rearranging the aquitard-drainage model time constant equation, utilizing the observed seasonal lag times, and then by the direct use of the estimated aquitard elastic skeletal specific storage and vertical hydraulic conductivity values (Table 9). The hydraulic diffusivity values were all nearly identical matches for each aquitard, which validates the estimated seasonal signal elastic skeletal specific storage values for the aquitards. If the elastic skeletal specific storage values were not valid, estimates of the hydraulic diffusivity determined from it would not have matched to the hydraulic diffusivity determined using the hydrodynamic lag times.

The estimated aquitard parameters also fall within the reasonable range of values determined from past studies conducted at sites in Las Vegas and Las Vegas Valley (Harrill, 1976; Waichler and Cochran, 1991), California (Riley, 1969; Sneed and Galloway, 2000), and Arizona (Helm, 1974, 1975) (Table 6, 8). The aquitard elastic skeletal specific storage values (Figure 12) are about one magnitude smaller than Pavelko's (2004) optimal values (Table 6) while the vertical hydraulic conductivity values are a few magnitudes larger (Table 7, 8). The reasonable range provided by Pavelko (2004) for the vertical hydraulic conductivity had nearly four orders of magnitude between the upper and lower limit. The estimated seasonal signal vertical hydraulic conductivity values may be a few magnitudes larger than Pavelko's (2004) optimal value but the difference in magnitudes is within reason.

However, real world complexities must be simplified into idealized scenarios to model an aquifer-system. Such simplifications can have an effect on estimated parameter values (Mercer and Faust, 1980). Pavelko's (2004) modeling of the aquifer-system may contribute to the magnitude differences observed between Pavelko's (2004) optimal values and the estimated values calculated using the seasonal signal due to the simplifications made and the fact that the optimal estimates are values for the aquifer and aquitard units, instead of the individual layers.

4.3 DECADAL SIGNAL

The use of a stress-strain plot provided an estimate for the Lorenzi site aquitard unit average inelastic skeletal specific storage that is one order of magnitude smaller than Pavelko's (2004) optimal estimate (Table 11) and correlates well with the estimated seasonal signal aquitard elastic skeletal specific storage values (Figure 12). Riley's (1969) graphical calculation has been used to determine numerous aquitard elastic and inelastic skeletal specific storage values for all types of aquifer-system arrangements. Stress-strain graphs have been created using

extensometer and hydrograph data (Cleveland, Bravo, & Rogers, 1992) but can also be created using InSAR and GPS technology (Burbey, 2001). With the increased availability of compaction data, stress-strain plots have become a typical method for estimating aquitard storage parameters.

The relationship of the average inelastic skeletal specific storage to Pavelko's (2004) optimal estimate and the aquitard elastic skeletal specific storage values may be the result of the amount of caliche found within the aquitard layers. In the section 1.2.1 Geologic Settings, it was stated that the fine-grained alluvium can be found as well-cemented, essentially impermeable caliche that is distributed randomly as horizons up to a meter thick (Bell, 1981). The formation of caliche requires pore spaces to be filled with calcium carbonate which cements sediment grains together (Schlesinger, 1985). The inelastic skeletal specific storage of an aquitard is controlled by the compressibility of the aquitard skeletal (grain) matrix therefore a reduction in pore space causes a reduction in compressibility (Terzaghi, 1925, 1943). The less compressible the aquitard units are the closer the average inelastic skeletal specific storage will be to the aquitard elastic skeletal specific storage values. In addition, lesser aquitard compressibility results in smaller inelastic skeletal specific storage values as well.

Individual aquitard inelastic skeletal specific storage values could not be determined because of the lack of suitable inelastic response trends for the stress-strain plots of each individual aquifer. Other attempts made to determine individual aquitard inelastic skeletal specific storage values resulted in erroneous values and were not included in this paper for brevity. The estimated aquitard unit average inelastic skeletal specific storage is thought to be tainted by the aquitard elastic skeletal specific storage values since the increasing water-levels eventually lead to the lowering of the effective stress below the preconsolidation stress. However, the water-levels began to rise for only the last few years of the record, thus the water-

level impact on the slope of the decadal stress-strain plot and its effect on the calculation of the aquitard inelastic skeletal specific storage values is considered to be relatively minimal.

4.4 PRINCIPAL COMPONENTS ANALYSIS

The results of all the principal components analyses indicate that PCA cannot detect the three temporal signals. Besides confirming the inverse relationship between water-level drawdown and subsidence (Table 12), PCA does not seem to yield any results relevant to the Lorenzi site aquifer-system. The statistical method PCA was chosen to evaluate the Lorenzi site data based on the successful application of PCA to multi-decadal InSAR-derived ground deformation data taken from Santa Clara Valley, California in Chaussard et al.'s (2014) study to predict hydraulic head changes and characterize aquifer-system and fault properties.

Using PCA Chaussard et al. (2014) was able to identify three principal components that corresponded to ground deformation related to three temporal scales. The first principal component explained over 70% of the variance in the data and correlated to long-term uplift due to delayed poroelastic rebound of aquitards in Santa Clara Valley (Chaussard et al., 2014). Poroelastic rebound describes the uplift that occurs when pore pressure in an aquifer-system is regained (Allen and Mayuga, 1969). The second and third principal components explained around 20% of the variance and corresponded to seasonal uplift, due to rainfall events, and delayed uplift, which occurred around 100 days after the rainfall events related to PC2, respectively (Chaussard et al., 2014).

Although Chaussard et al.'s (2014) study used similar ground deformation data, it was also spatially distributed across two basins within Santa Clara Valley. The uplift in PC1 was observed across the two basins, PC2's uplift encompassed most of the confined aquifer within Santa Clara Valley, and PC3's uplift was limited to a region around 3 km wide (Chaussard et al.,

2014). The addition of spatially distributed ground deformation data to the study of the aquifer-system at the Lorenzi site could potentially allow for the detection of the three temporal signals. However, this spatial analysis of deformation was beyond the scope of work described here.

CHAPTER 5: CONCLUSIONS

From the single cumulative compaction record and corresponding nested water-level data, deconvolved into temporal components, aquitard elastic specific storage and vertical hydraulic conductivity were determined for each of the three aquitards present at the Lorenzi site and aquifer elastic specific storage and horizontal hydraulic conductivity were determined for both the middle and deep aquifers. An average inelastic skeletal specific storage was also estimated for the cumulative aquitard units at the Lorenzi site. Unfortunately, the presence of the three temporal signals could not be detected by the statistical analysis PCA.

Although some assumptions were made the similarities between nearly all of the estimated parameters and the values determined from previous studies were high. A cumulative compaction record is difficult to obtain, InSAR derived ground deformation data is comprised of only one measurement every three-six months, but when the precision measurements are analyzed they lead to precise aquifer-system parameters. As the precision of aquifer-system parameters increase so does the ability to manage groundwater efficiently and effectively. Known aquifer-system parameters can be used by water managers in site-specific aquifer-system models to estimate sustainable pumping rates and pumping schedules, such as the use of diurnal or seasonal pumping. The demand for water resources is only going to intensify as time goes by and water management practices are the only viable defense against land subsidence and the various expensive problems that go along with it.

Overall, the analytical analysis of the deconvolved Lorenzi site data record produced very specific aquifer-system parameters, compared to the generalized aquifer-system unit parameters estimated from Pavelko's (2004) one-dimensional numerical model, however more effort was required to determine the exact analyses necessary to estimate the hydraulic parameters from each temporal signal. Although the accuracy of the observational data record was a limitation for both, the analytical analysis was also dependent on pumping well data while Pavelko's (2004) one-dimensional model was dependent on past historical ground deformation that occurred at the Lorenzi site. The pumping well data proved insufficient and the historical ground deformation was unknown which resulted in assumptions having to be made in both the analytical analysis and one-dimensional numberical model methods.

Pavelko's (2004) one-dimensional numerical model precluded its ability to calculate aquifer hydraulic conductivity values due to the nature of the modeling simulation. The analytical analysis method was able to determine hydraulic parameters for nearly each individual aquifer and aquitard layer using a variety of analyses. The ability to utilize different approaches to analyze each temporal signal is the greatest strength of the analytical analysis method. The one requirement for the analytical analysis method that must always be met and could limit the usefulness of this method is the presence of periodic signals within both the water-level and subsidence data records. If periodic signals are not present, an alternative analysis method must be utilized, such as a one-dimensional numerical model.

5.1 FUTURE RESEARCH

The next step with this research would be to use the estimated parameters determined from each temporal signal as input values for a model on the Lorenzi site aquifer-system. If the estimated parameters truly represent the aquifer-system at the Lorenzi site the model should

recreated the long-term total compaction record. This would be a final check on the validity of determining aquifer-system parameters from a single cumulative compaction record and corresponding nested water-level data deconvolved into temporal components.

Although the estimated parameters, in most cases, fall within or are of the same magnitude as the reasonable range of values reported in Pavelko (2004) most of the assumptions made during the calculations of the estimated parameters could be removed, reducing the number of unknowns. A better idea of how pumping occurs at the LVVWD well field could determine a better estimate for partitioning pumping rates. That could reduce, or eliminate, the need for the range of elastic skeletal specific storage and horizontal hydraulic conductivity values needed to be estimated for the aquifers.

Also, knowing which aquifers are pumped by each well would help determine the best method for solving the daily pumping test. Single-layered leaky aquifers were assumed for the pumping test but a solution, derived by Papadopulos (1966), for unsteady-state flow to a well that fully penetrates an aquifer-system, and pumps both confined aquifers at the same time, also exists and may be more realistic. Solutions are available for many other pumping tests but without more information about the pumping wells, assumptions must be made.

Finally, the addition of spatially distributed ground deformation data to the Lorenzi site extensometer data would improve the chances of obtaining significant results from PCA. Extensive multi-decadal InSAR-derived ground deformation data is already available for Las Vegas Valley (Bell et al., 2002) and could easily be used with PCA to not only detect the temporal signals but also determine in which regions each temporal signal is presently occurring. Since PCA has already successfully detected delayed ground deformation trends (Chaussard et

al., 2014) it could also be used to verify the hydrodynamic time lag determined from the seasonal signal.

REFERENCES

Abdi, H., Williams, L.W., 2010, Principal components analysis: WIREs Computational Statistics, v. 2, p. 433-456.

Allen, D.R., Mayuga, M.N., 1969, The mechanics of compaction and rebound, Wilmington Oil Field, Lon Beach, California, USA: International Hydrological Decade, symposium on land subsidence, Tokyo, Japan.

Amelung, F., Galloway, D.L., Bell, J.W., Zebker, H.A., and Laczniak, R.J., 1999, Sensing the ups and downs of Las Vegas: InSAR reveals structural control of land subsidence and aquifer-system deformation: Geology, v. 27, no. 6, p. 483-486.

Bell, J.W., 1981, Subsidence in Las Vegas Valley: Nevada Bureau of Mines and Geology Bulletin 95, 84 p.

_____ 1997, Las Vegas Valley: Land subsidence and fissuring due to ground-water withdrawal: U.S. Geological Survey Nevada Bureau of Mines and Geology, last accessed February 2016 at: <http://geochange.er.usgs.gov/sw/impacts/hydrology/vegas_gw/>

Bell, J.W., Price, J.G., 1991, Subsidence in Las Vegas Valley, 1980-91 Final Project Report: Nevada Bureau of Mines and Geology Open-File Report 93-4.

Bell, J.W., Amelung, F., and Ramelli, A.R., 2000, Land subsidence in Las Vegas, Nevada, USA: new geodetic data reveal localized spatial patterns, structural controls, and reduced rates, in Carbognin, Laura, Gambolati, Giuseppe, and Johnson, A.I., eds., Land subsidence v. II: Proceedings of the Sixth International Symposium on Land Subsidence, Ravenna, Italy, p. 127-138.

Bell, J.W., Amelung, F., Ramelli, A.R., and Belewitt, G., 2002, Land subsidence in Las Vegas, Nevada, 1935-2000: new geodetic data show evolution, revised spatial patterns, and reduced rates: Environmental & Engineering Geoscience, v. VIII, no. 3, p. 155-174.

Burbey, T.J., 1995, Pumping and water-level change in the principal aquifer of Las Vegas Valley, Nevada, 1980-90: Nevada Division of Water Resources Information Report 34, 224 p.

_____ 2002, The influence of faults in basin-fill deposits on land subsidence, Las Vegas Valley, Nevada, USA: Hydrogeology Journal, v. 10, p. 525-538.

_____ 2003, Use of time-subsidence data during pumping to characterize specific storage and hydraulic conductivity of semi-confining units: Journal of Hydrology, v. 281, p. 3-22.

_____ 2005, Use of vertical and horizontal deformation data with inverse models to

quantify parameters during aquifer testing: Proceedings of the Seventh International Symposium on Land Subsidence, Shanghai China

Carpenter, E., 1915, Ground water in southeastern Nevada: U.S. Geological Survey Water-supply Paper 365, 86 p.

Chaussard, E., Burgmann, R., Shirzaei, A., Fielding, E.J., and Baker, B., 2014, Predictability of hydraulic head changes and characterization of aquifer system and fault properties from InSAR-derived ground deformation: Journal of Geophysical Research: Solid Earth, v.119, 19 p.

Cleveland, T.G., Bravo, R., Rogers, J.R., 1992, Storage Coefficients and Vertical Hydraulic Conductivities in Aquitards Using Extensometer and Hydrograph Data: GroundWater, v. 30, no. 5, p. 701-708.

Cooper, H., Jacob, C., 1946. A generalized graphical method for evaluation formation constants and summarizing well-field history: Transactions of the American Geophysical Union 27, 526-534.

Delage, P., Lefebvre, G., 1984, Study of the structure of a sensitive Champlain clay and of its evolution during consolidation: Canadian Geotechnical Journal, v. 21, p. 21-35.

Domenico, P.A., Stephenson, D.A., and Maxey, G.B., 1964, Ground water in Las Vegas: Nevada Department of Conservation and Natural Resources: Water Resources Bulletin 29, 53 p.

Domenico, P.A., Mifflin, M.D., and Mindling, A.L., 1996, Geologic controls on land subsidence in Las Vegas Valley: Proceedings, Fourth Annual Engineering Geologist and Soil Engineering Symposium: Moscow, Idaho, p. 113-121.

Donovan, D.J., Katzer, T., 2000, Hydrologic implications of greater groundwater recharge to Las Vegas Valley, Nevada: Journal of the American Water Resources Association, v. 36, no. 5, p. 1134-1148.

Epstein, V.J., 1987, Hydrologic and geologic factors affecting land subsidence near Eloy, Arizona: U.S. Geological Survey Water-Resources Investigations Report 87-4143, 28 p.

Freeland, J., 2013, Soil Anisotropy: Mechanisms and Hydrologic Consequences: American Geophysical Union, last accessed May 19 at: <http://blogs.agu.org/terracentral/2013/07/01/soil-anisotropy-mechanisms-and-hydrologic-consequences/>

Freeze, R.A., Cherry, J.A., 1979, Groundwater: Englewood Cliffs, New Jersey, Prentice-Hall, p. 55.

Galloway, D.L., Jones, D.R., and Ingebritsen, S.E., 2000, Measuring land subsidence

from space: U.S. Geological Survey Fact Sheet 051-00, 4 p.

Godin, G., 1972, The Analysis of Tides, University of Toronto Press, Toronto, p. 62-66.

Hanson, R.T., 1989, Aquifer-system compaction, Tucson Basin and Avra Valley, Arizona: U.S. Geological Survey Water Resources Investigations Report 88-4172, 69 p.

Harrill, J.R., 1976, Pumping and ground-water storage depletion in Las Vegas Valley, Nevada, 1955-74: Nevada Department of Conservation and Natural Resources, Water Resources Bulletin 44, 70 p.

Helm, D.C., 1974, Evaluation of stress-dependent aquitard parameters by simulating observed compaction from known stress history: Berkeley, California, University of California, doctoral dissertation, 175 p.

_____ 1975, One-dimensional simulation of aquifer-system compaction near Pixley, California, 1. Constant Parameters: Water Resources Research, v. 11, no. 3, p. 465-478.

_____1984, Field-based computational techniques for predicting subsidence due to fluid withdrawal: Geological Society of America, Reviews in Engineering Geology, v. VI, 22 p.

Hoffmann, J., Zebker, H.A., Galloway, D.L., and Amelung, F., 2001, Seasonal subsidence and rebound in Las Vegas Valley, Nevada, observed by synthetic aperture and radar interferometry: Water Resources Research, v. 37, no. 6, p. 1551-1566.

Holzer, T.L., 1998, History of the aquitard-drainage model, in Borchers, J.W., ed., Land subsidence case studies and current research: Proceedings of the Dr. Joseph F. Poland symposium on land subsidence, Association of Engineering Geologists Special Publication no. 8, p. 7-12.

Hsieh, P.A., Bredehoeft, J.D., Farr, J.M., 1987, Determination of Aquifer Transmissivity From Earth Tide Analysis: Water Resources Research, vo. 23, no. 10, p. 1824-1832.

Jeng, D.I., 1998, A ground-water flow and land subsidence model of Las Vegas Valley, Nevada-a converted MODFLOW model: Reno, University of Nevada, M.S. Thesis, 123 p.

Kruseman, G.P., Ridder, N.A., 1994, Analysis and Evaluation of Pumping Test Data, 2nd ed., The Netherlands, International Institute for Land Reclamation and Improvement, 377 p.

Lahey Computer Systems, Inc., 2002, FORTRAN 95 PRO, version 5.7. Computer Software. Incline Village, Nevada. Disk.

Leake, S.A., Prudic, D.E., 1991, Documentation of a computer program to simulate aquifer-system compaction using the modular finite-difference ground-water flow model: U.S. Geologic Survey Techniques of Water-Resources Investigations 06-A2, 68 p.

Malmburg, G.T., 1964, Land subsidence in Las Vegas Valley, Nevada, 1935-63: Nevada Department of Conservation and Natural Resources Water Resources –Information Report 5, 10 p.

_____ 1965, Available water supply of the Las Vegas ground-water basin, Nevada: U.S. Geological Survey Water-Supply Paper 1780, 116 p.

Maxey, G.B., Jameson, C.H., 1948, Geology and water resources of Las Vegas, Pahrump, and Indian Spring Valleys, Clark and Nye Counties, Nevada: Nevada State Engineer, Water Resources Bulletin 5, 121p.

Mercer, J.W., Faust, C.R., 1980, Ground-Water Modeling: An Overview: Groundwater, v. 18, no. 2, p. 108-115.

Mindling, A.L., 1965, An investigation of the relationship of the physical properties of fine-grained sediments to land subsidence in Las Vegas Valley, Nevada: University of Nevada, Reno, unpublished Master's Thesis, 90 p.

_____ 1971, A summary of data relating to land subsidence in Las Vegas Valley: University of Nevada, Desert Research Institute, 55 p.

Morgan, D.S., Dettinger, M.D., 1996, Ground-water conditions in Las Vegas Valley, Clark County, Nevada, Part 2, Hydrogeology and simulation of ground-water flow: U.S. Geological Survey Water-Supply Paper 2320-B, 124 p.

National Research Council, 1991, Mitigating losses from land subsidence in the United States: Washington, D.C.: National Academy Press, 58 p.

Okuyan, M.N., 2000, Modelling land subsidence due to groundwater pumping/recharging in the Las Vegas Valley: Las Vegas, University of Nevada, M.S. Thesis, 91 p.

Papadopulos, I.S., 1966, Nonsteady flow to multi-aquifer wells: Journal Geophysical Research, v. 71, p. 4791-4797.

Pavelko, M.T., Wood, D.B., and Laczniak, R.J., 1999, Las Vegas Valley, Nevada – Urbanization: Gambling with water in the desert, in Galloway, D., Jones, D., and Ingebritsen, S., eds., Land subsidence in the United States: U.S. Geological Survey Circular 1182, p. 49-64.

Pavelko, M.T., 2000, Ground-water and aquifer-system-compaction data from the Lorenzi Site, Las Vegas, Nevada, 1994-99: U.S. Geological Survey Open-File Report 00-362, 26 p.

_____ 2003, Application of nonlinear regression methods to estimate hydraulic properties that control vertical aquifer-system deformation at the Lorenzi site, Las Vegas, Nevada, in Prince, K.R., and Galloway, D.L., eds., U.S. Geological Survey Subsidence Interest Group conference, proceedings of the technical meeting, Galveston, Texas, p. 57-62.

_____ 2004, Estimates of hydraulic properties from a one-dimensional numerical model of vertical aquifer-system deformation, Lorenzi Site, Las Vegas, Nevada: U.S. Geological Survey Water-Resources Investigations Report 03-4083, 35 p.

Plume, R.W., 1989, Ground-water conditions in Las Vegas Valley, Clark County, Nevada, Part 1, Hydrogeologic framework: U.S. Geological Survey Water-Supply Paper 2320-A, 15 p.

Poland, J.F., Lofgren, B.E., and Riley, F.S., 1972, Glossary of selected terms useful in studies of the mechanics of aquifer systems and land subsidence due to fluid withdrawal: U.S. Geological Survey Water-Supply Paper 2025, 9 p.

Pope, J.P., Burbey, T.J., 2004, Multiple-Aquifer Characterization from Single Borehole Extensometer Records: GroundWater, v. 42, no. 1, p. 45-58.

R Core Team, 2012, R: A language and environment for statistical computing: R Foundation for Statistical Computing, Vienna, Austria. ISBN 3-900051-07-0, last accessed May 17, 2015 at <http://www.R-project.org/>

Rhudy, M., Bucci, B., Vipperman J., Abraham, B., 2009, Microphone Array Analysis Methods Using Cross-Correlations: Proceedings ASME Internationsal Mechanical Engineering Congress, Lake Buena Vista, Florida.

Riley, F.S., 1969, Analysis of borehole extensometer data from central California: International Association of Scientific Hydrology Publication 89, p. 423-431.

Rudolph, D.L., Frind, E.O., 1991, Hydraulic Response of Highly Compressible Aquitards During Consolidation: Water Resources Research, v. 27, no. 1, p. 17-30.

Smith, L.I., 2002, A tutorial on Principal Components Analysis, last accessed March 25, 2016 at: <http://www.cs.otago.ac.nz/cosc453/student_tutorials/principal_components.pdf>

Sneed, M., Galloway, D.L., 2000, Aquifer-system compaction and land subsidence: mearsurements, analyses, and simulations—the Holly Site, Edwards Air Force Base, Antelope Valley, California: U.S. Geological Survey Water Resources Investigations Report 00-4015, 65 p.

Terzaghi, K., 1925, Principles of soil mechanics: IV; settlement and consolidation of

clay: Engineering News Record, v. 95, no. 3, p. 874-878.

_____ 1943, Theoretical soil mechanics: New York, Wiley, 510 p.

Tolman, C.F., Poland, J.F., 1940, Ground-water infiltration, and ground-surface recession in Santa Clara Valley, Santa Clara County, California: Transactions American Geophysical Union, v. 21, p. 23-34.

United Nations Educational, Scientific and Cultural Organization, 2016, What is Land Subsidence?, UNESCO, last accessed June 2, 2016 at <http://landsubsidence-unesco.org/content/what-land-subsidence>

U.S. Geologic Survey, 1999, Land Subsidence in the United States: U.S. Geologic Survey Circular 1182, 177 p.

_____ 2013, Land Subsidence, U.S. Geologic Survey, last accessed March 1, 2016 at: <http://water.usgs.gov/ogw/subsidence.html>

_____ 2016, Groundwater for USA: Water Levels, U.S. Geologic Survey, last accessed February 2016 at: <http://nwis.waterdata.usgs.gov/nwis/gwlevels?>

Waichler, S.R., Conchran, G.F., 1991, Modelling and prediction of land subsidence in Las Vegas Valley, Nevada: University of Nevada, Desert Research Institute: Water Resources Center Publication 41133, 30 p.

Waterloo Hydrogeologic Inc., 2014, AquiferTest Pro, v. 2014.1, build 4.6.0.2, Ontario, Canada, Nova Metrix Ground Monitoring Ltd.

Whipkey, R.Z., Kirkby, M.J., 1978, Flow within Soil. In M.J. Kirkby Hillslope Hydrology: New York, John Wiley & Sons, p. 1121-1144.

Yan, T., 2007, Effects of delayed drainage on subsidence modeling and parameter estimation: Blacksburg, Virginia, Polytechnic Institute and State University, M.S. Thesis, 94 p.

Zhang, M., Burbey, T.J., 2016, Hydrological Processes (accepted not currently typeset).

APPENDICES

APPENDIX A

Groundwater for USA: Water Levels (USGS, 2016)

Agency	Site Number	Site Name
USGS	361410115142601	212 S20 E60 02CCBB1 USGS-PZD
USGS	361410115142602	212 S20 E60 02CCBB2 USGS-PZM
USGS	361410115142603	212 S20 E60 02CCBB3 USGS-PZS
USGS	361410115142604	212 S20 E60 02CCBB4 USGS-Ext1

National Aquifer: N100BSNRGB County: Clark

APPENDIX B

FORTRAN Low Pass Filter Code

```
!     Last change:  TJB   9 Jul 2012    3:45 pm
PROGRAM filter
!
! Purpose:
! This program uses both a smoothing process and low-pass filter to extract both
! noise and trends from the tidal signal in water-level data. The filter is developed
! by Godin (1972, p. 62-66).
!
!      Date          Programmer           Revisions
!      ====          ==========           =========
!      8-19-08       T.J. Burbey          original code
!      7-9-12        T.J. Burbey          revised for sub data filtering
!
!_____________________________________________________________________________
__
!
IMPLICIT NONE
INTEGER:: M,n                    ! M=total number of observed values, n= dt multiplier
REAL, DIMENSION(6000):: jtime,time   ! time corresponding to z(j*dt)
REAL, DIMENSION(6000):: z            ! observed value z(t)
REAL, DIMENSION(6000):: znew         ! output of z values
REAL, DIMENSION(6000):: X,Y,Z0       ! summation values used in algorithm
REAL:: xsum                      ! temporary value for summation
INTEGER:: i,j,k                  ! loop counters
CHARACTER(LEN=20):: filename1        ! file name containing z(t) data
CHARACTER(LEN=20):: outfile          ! output file name with new znew(t) data
CHARACTER(LEN=1) dummy               ! dummy variable
INTEGER:: tdays                    ! total days
INTEGER:: jd                     ! julian days
INTEGER:: d1940                    ! days since 1940
REAL:: hpzs_ft                   ! shallow piez (ft)
REAL:: hpzs_m                     ! shallow piez (m)
REAL:: hpzm_ft                    ! middle piez (ft)
REAL:: hpzm_m                      ! middle piez (m)
REAL:: hpzd_ft                   ! deep piez (ft)
REAL:: hpzd_m                     ! deep piez (m)
REAL:: sub_mm                      ! subsidence (mm)
REAL:: sub_ltrend                 ! long-term subsidence trend


! Read in information
WRITE(*,*) "Enter filename containing the data"
```

```
read (*,*) filename1
OPEN(UNIT=5, FILE=filename1, STATUS='old', ACTION='read')
WRITE(*,*) "number of z values in the file?"
READ(*,*) M
WRITE(*,*) "Enter filter value = number of data points being averaged"
READ(*,*) n
WRITE(*,*) "What is the name of the output file?"
READ(*,*) outfile
OPEN(UNIT=6, FILE=outfile, STATUS='replace', ACTION='write')

!Get the data
!Read the header first
READ(5,*) dummy
DO i=1,M-1
READ(5,*) tdays,jd,jtime(i),d1940,hpzs_ft,hpzs_m,hpzm_ft,hpzm_m,hpzd_ft,hpzd_m,&
sub_mm,sub_ltrend,z(i)
END DO

!Perform the algorithm of Godin (1972, p. 66)
! The first loop calculates X
DO k=1,M-n+1
  xsum=0.
  DO j=0,n-1
    xsum=xsum+z(j+k)
  END DO
!     IF(MOD(n,2)==0) then
!       time(k)=dt*(k+(n-1)/2)
!     Else
!       time(k)=dt*((k+n/2-1)+(k+n/2))/2
!     END if
  X(k)=xsum/n
END DO

! The second loop represents (A sub n) squared
do i=1,M-2*n+1
  xsum=0.
  do k=0,n-1
    xsum=xsum+X(k+i)
  end do
  Y(i)=xsum/n
end do

! The third loop represents (A sub n)squared*(A sub n+1)
do i=1,M-3*n+1
  xsum=0.
  do j=0,n
```

```
    xsum=xsum+Y(i+j)
  end do
  Z0(i)=xsum/(n+1)
  IF(MOD((3*n+1)/2,2)==1) then
    time(i)=jtime(i-1+(3*n+1)/2)
  else
    time(i)=0.5*(jtime(i-1+(3*n/2))+jtime(i-1+(3*n+2)/2))
  endif
end do

!Write out the results
do i=1,M-3*n+1
   WRITE(6,200) time(i), Z0(i)
end do
200 FORMAT(F10.4,10x,f12.6)

!Finish up
Stop
END PROGRAM
```

APPENDIX C

Determining which aquifers the constant pumping rate will be proportioned between, for use with AquiferTest Pro (Waterloo Hydrogeology Inc., 2014).

Aquifer	Average Head Change (m)	Total Head Change (%)
Shallow	0.03	0.74*
Middle	1	24.82
Deep	3	74.44
Total	**4.03**	**100**

*Pumping occurring in the shallow aquifer is considered negligible.

APPENDIX D

Partition of total compaction based on maximum head change observed for each aquifer in seasonal signal.

Aquifer	Maximum Head Change (m)	Total Head Change* (%)
Shallow Aquifer	6.48	16.36
Middle Aquifer	13.42	33.87
Deep Aquifer	19.72	49.77
Total	**39.62**	**100**

*Percent of total head change was partitioning factor.

Stress-strain plots of Shallow Aquifer for 12 seasonal cycle (years):

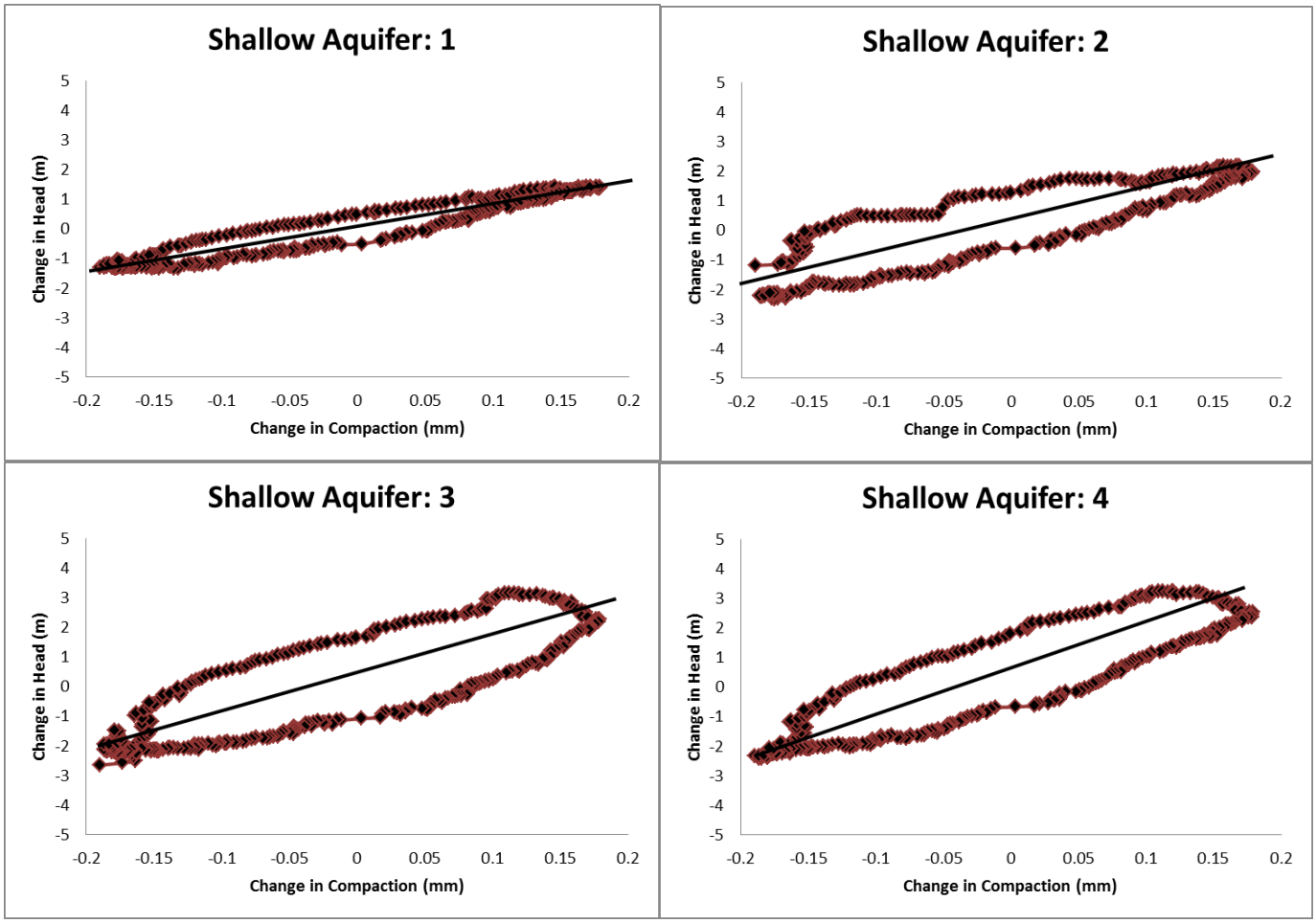

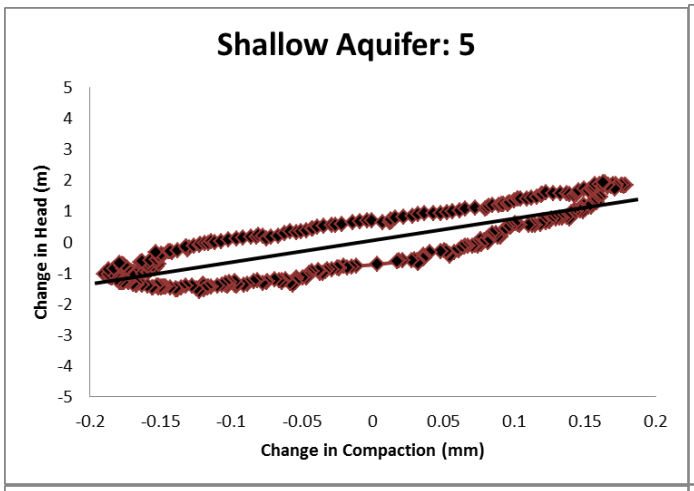
Shallow Aquifer: 5
Change in Head (m)
Change in Compaction (mm)

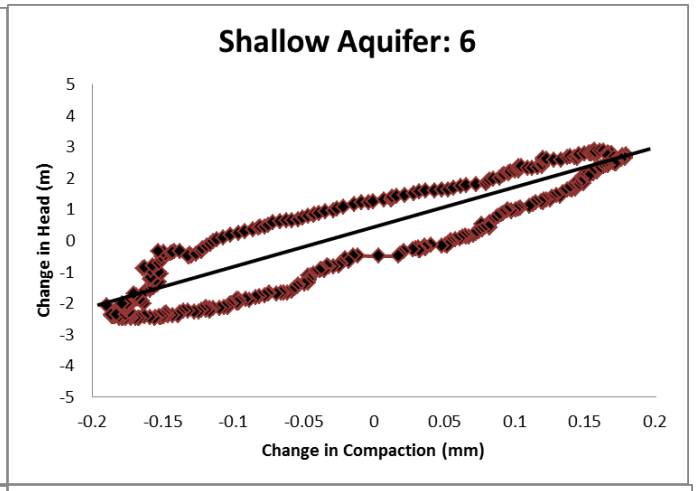
Shallow Aquifer: 6
Change in Head (m)
Change in Compaction (mm)

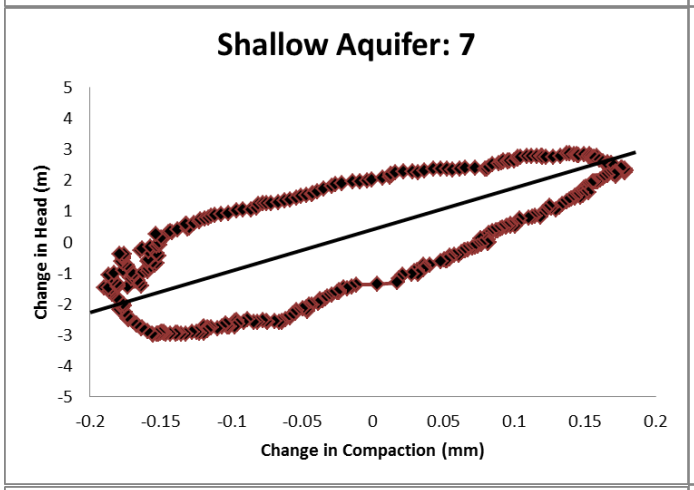
Shallow Aquifer: 7
Change in Head (m)
Change in Compaction (mm)

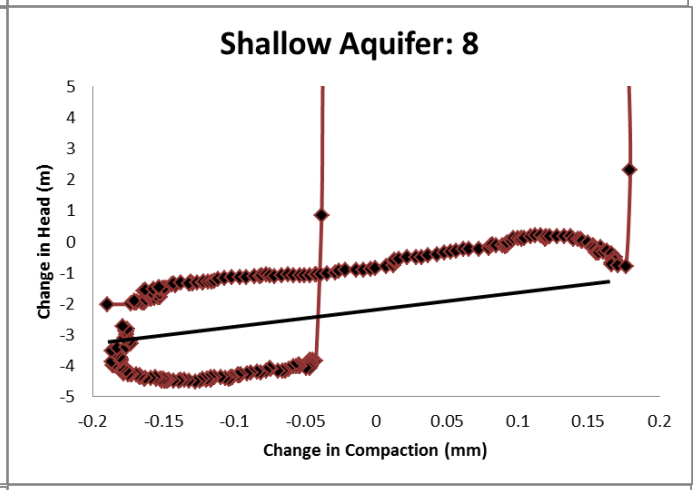
Shallow Aquifer: 8
Change in Head (m)
Change in Compaction (mm)

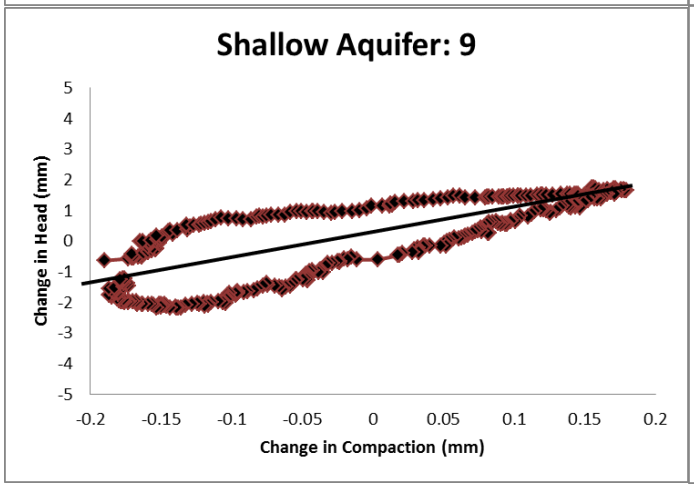
Shallow Aquifer: 9
Change in Head (mm)
Change in Compaction (mm)

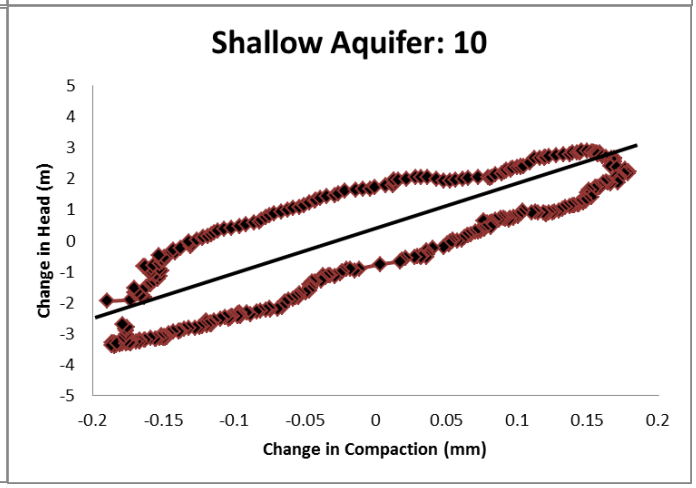
Shallow Aquifer: 10
Change in Head (m)
Change in Compaction (mm)

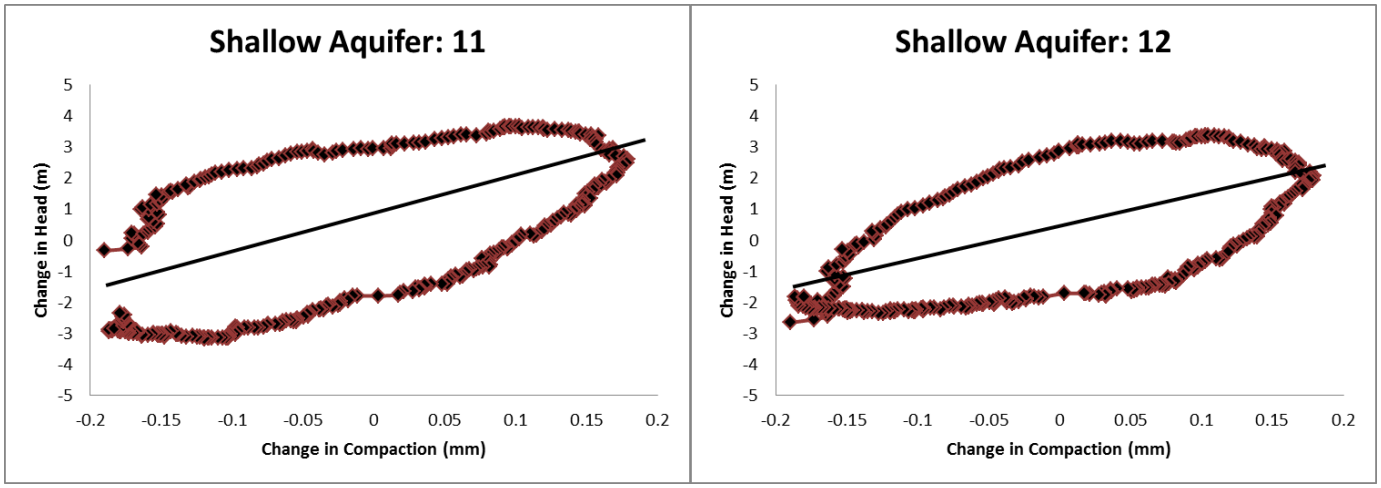

Stress-strain plots of Middle Aquifer for 12 seasonal cycle (years):

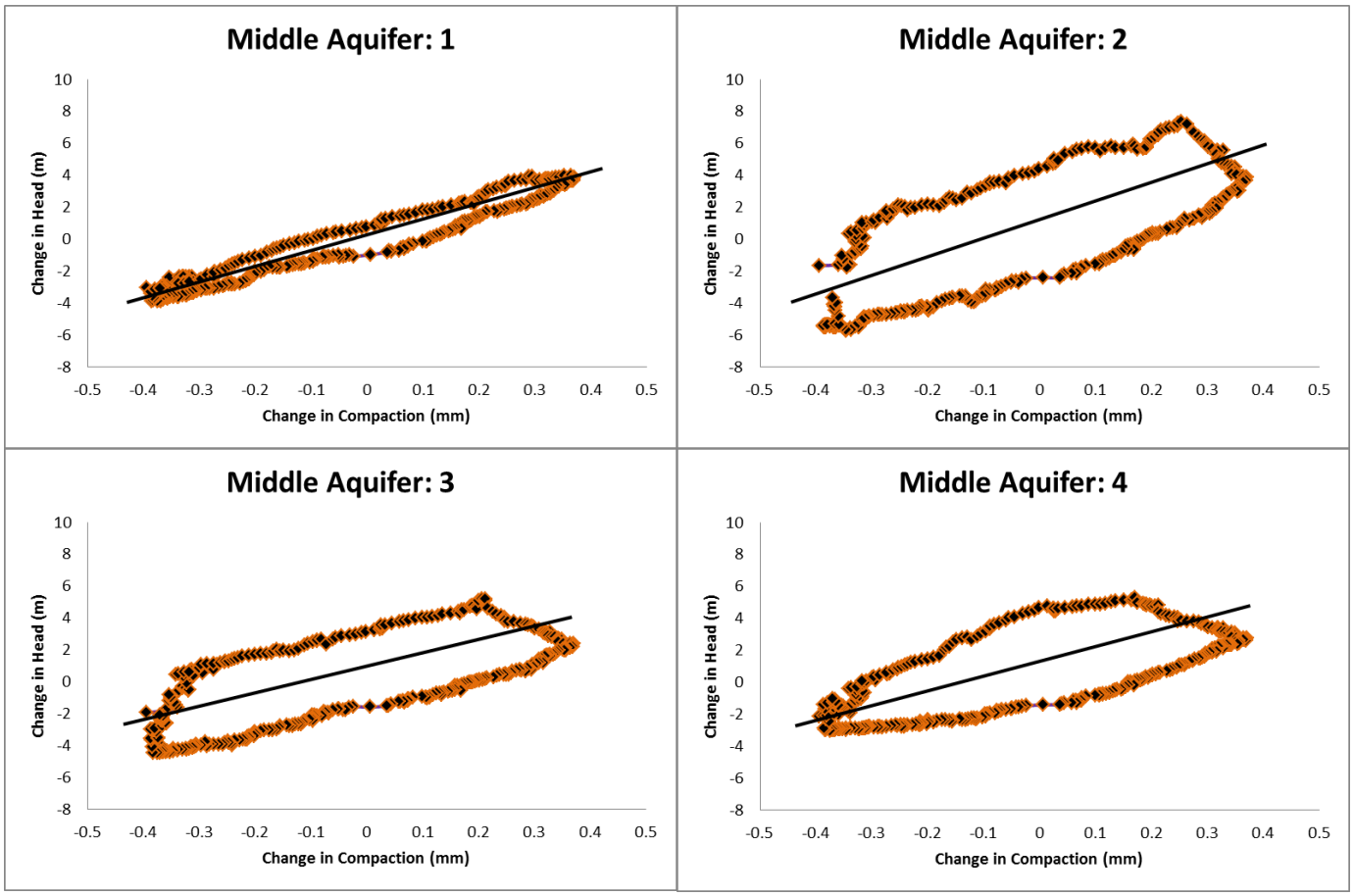

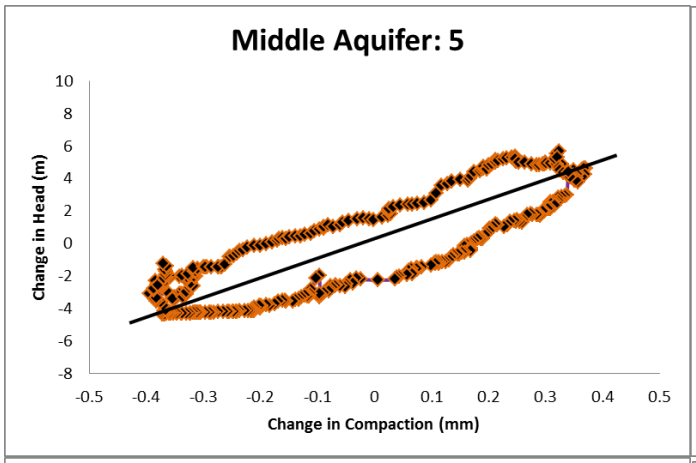
Middle Aquifer: 5
Change in Head (m)
Change in Compaction (mm)

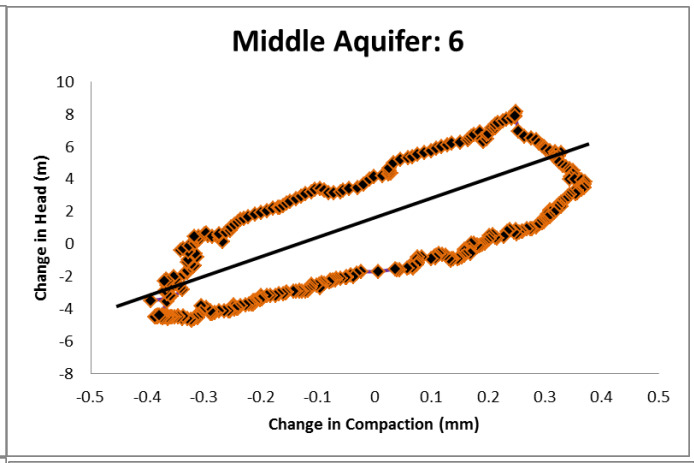
Middle Aquifer: 6
Change in Head (m)
Change in Compaction (mm)

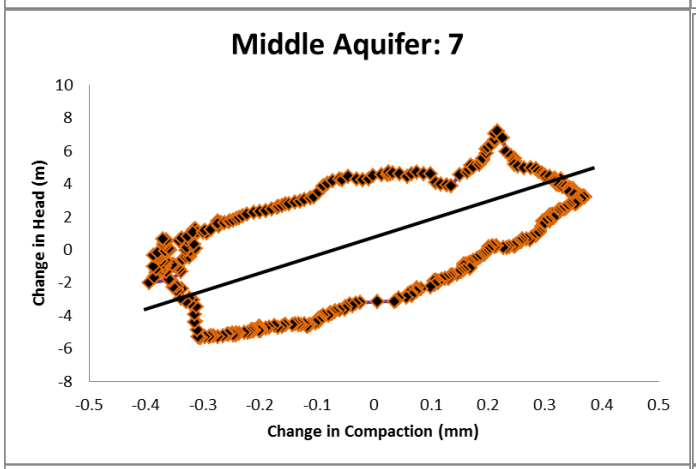
Middle Aquifer: 7
Change in Head (m)
Change in Compaction (mm)

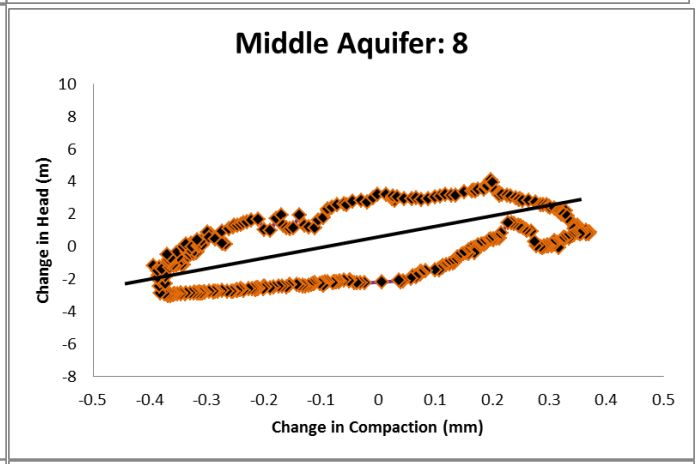
Middle Aquifer: 8
Change in Head (m)
Change in Compaction (mm)

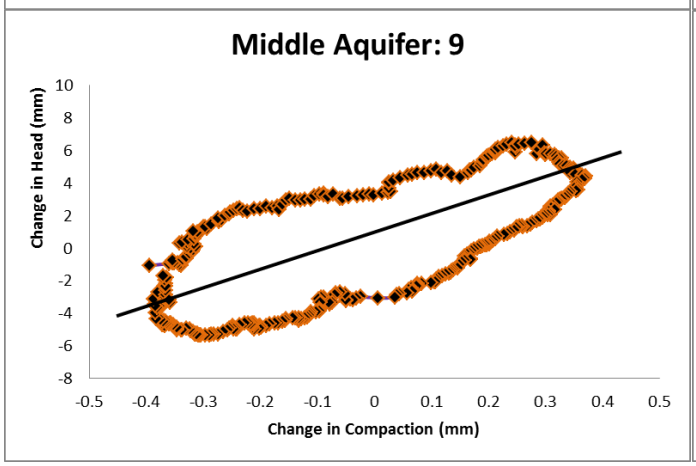
Middle Aquifer: 9
Change in Head (mm)
Change in Compaction (mm)

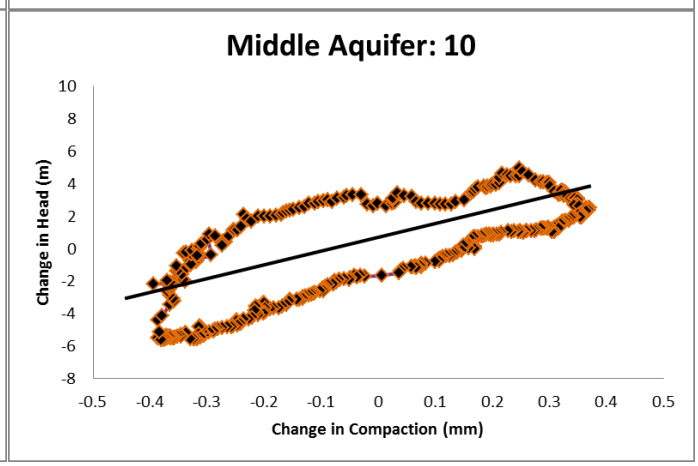
Middle Aquifer: 10
Change in Head (m)
Change in Compaction (mm)

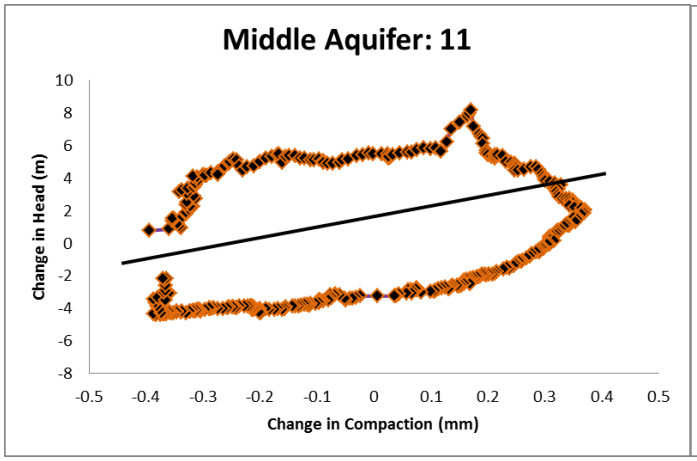

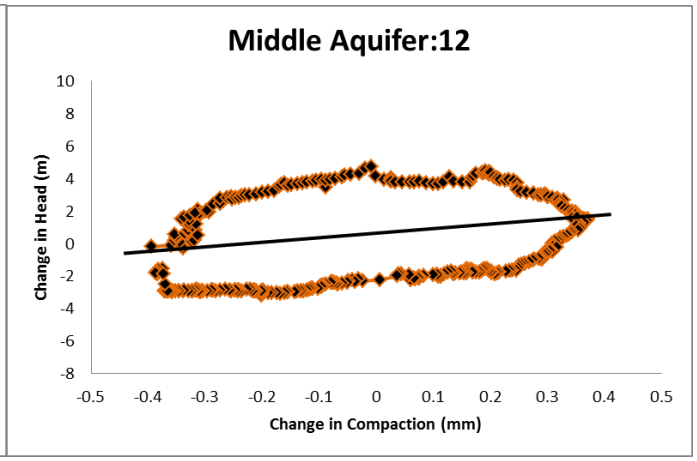

Stress-strain plots of Deep Aquifer for 12 seasonal cycle (years):

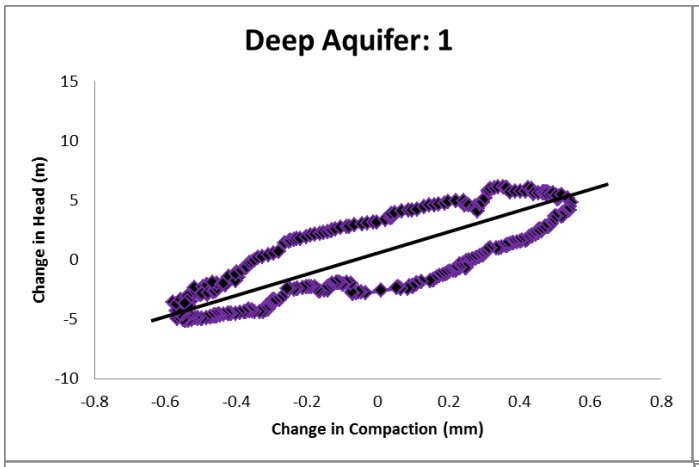

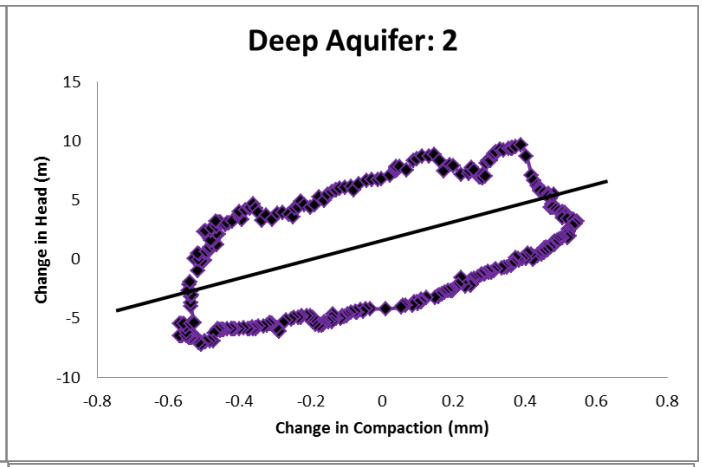

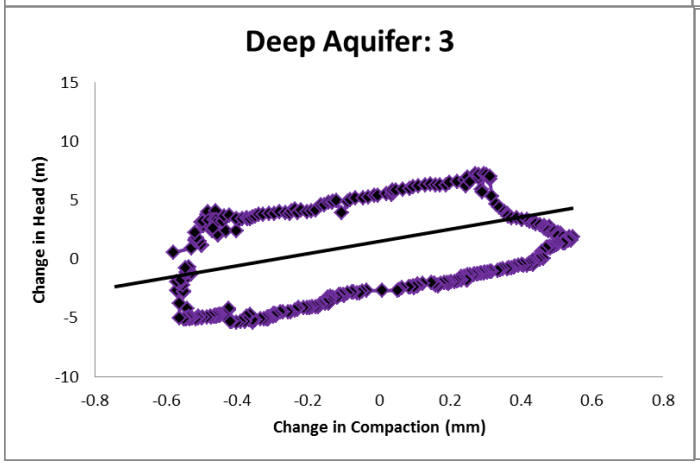

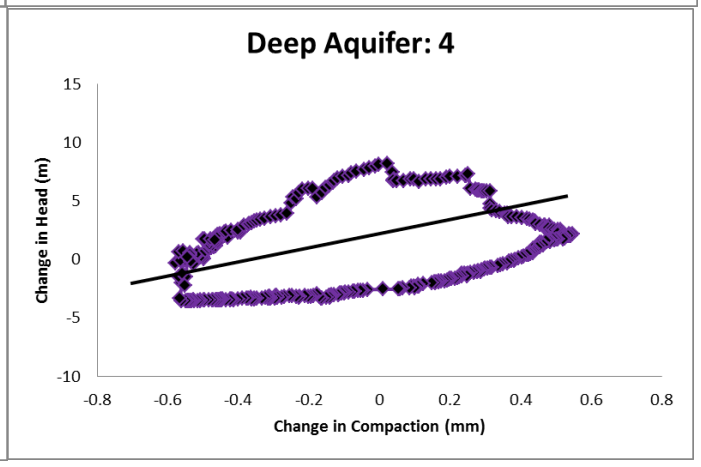

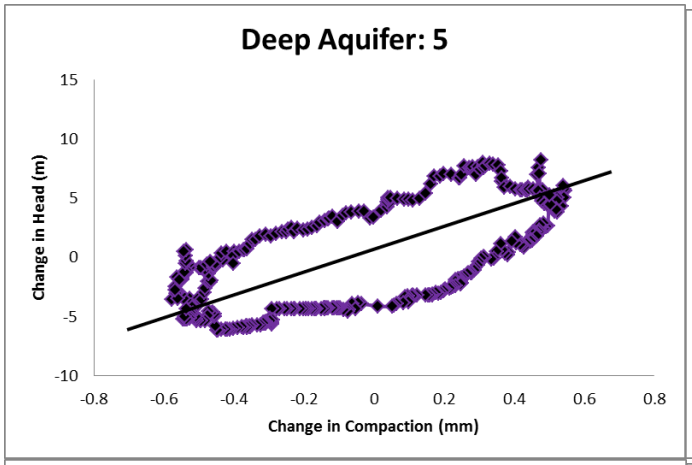
Deep Aquifer: 5
Change in Head (m)
15
10
5
0
-5
-10
-0.8
-0.6
-0.4
-0.2
0
0.2
0.4
0.6
0.8
Change in Compaction (mm)

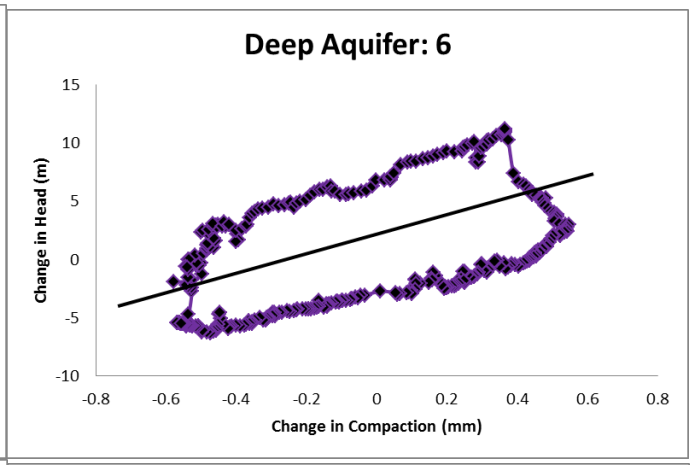
Deep Aquifer: 6
Change in Head (m)
15
10
5
0
-5
-10
-0.8
-0.6
-0.4
-0.2
0
0.2
0.4
0.6
0.8
Change in Compaction (mm)

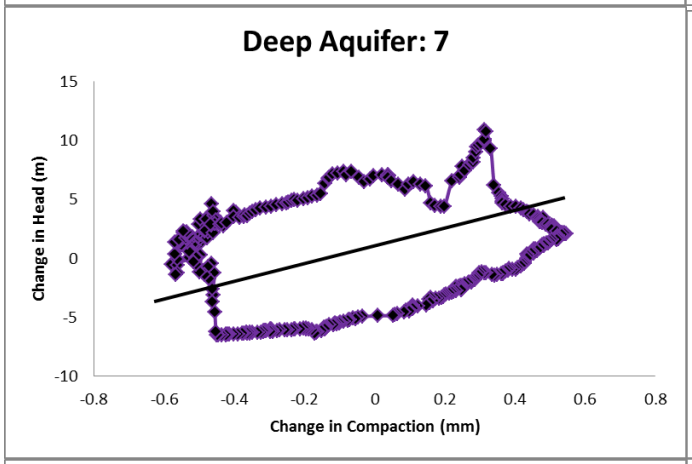
Deep Aquifer: 7
Change in Head (m)
15
10
5
0
-5
-10
-0.8
-0.6
-0.4
-0.2
0
0.2
0.4
0.6
0.8
Change in Compaction (mm)

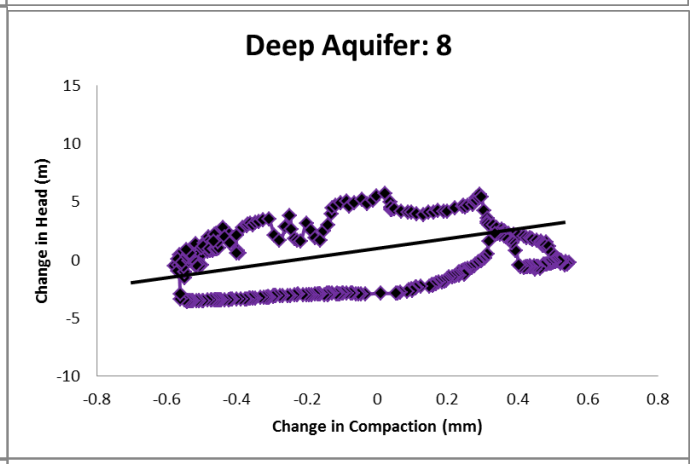
Deep Aquifer: 8
Change in Head (m)
15
10
5
0
-5
-10
-0.8
-0.6
-0.4
-0.2
0
0.2
0.4
0.6
0.8
Change in Compaction (mm)

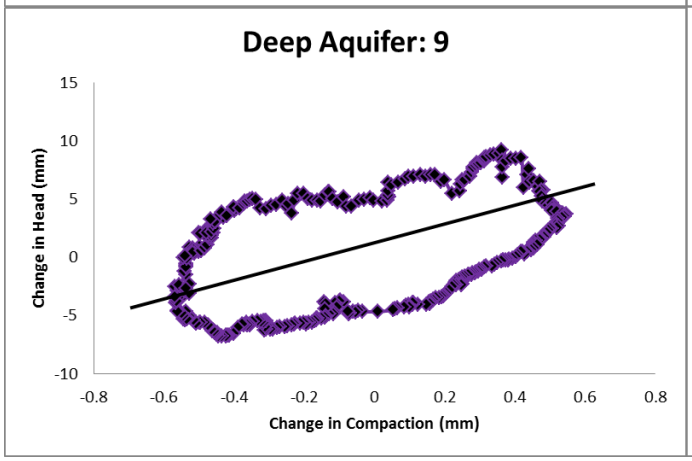
Deep Aquifer: 9
Change in Head (mm)
15
10
5
0
-5
-10
-0.8
-0.6
-0.4
-0.2
0
0.2
0.4
0.6
0.8
Change in Compaction (mm)

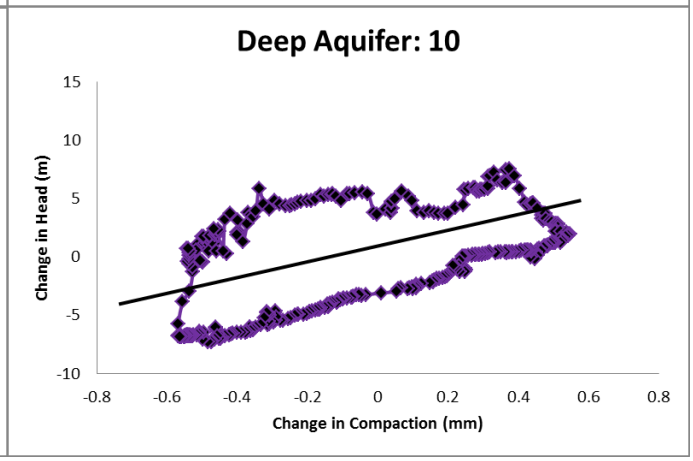
Deep Aquifer: 10
Change in Head (m)
15
10
5
0
-5
-10
-0.8
-0.6
-0.4
-0.2
0
0.2
0.4
0.6
0.8
Change in Compaction (mm)

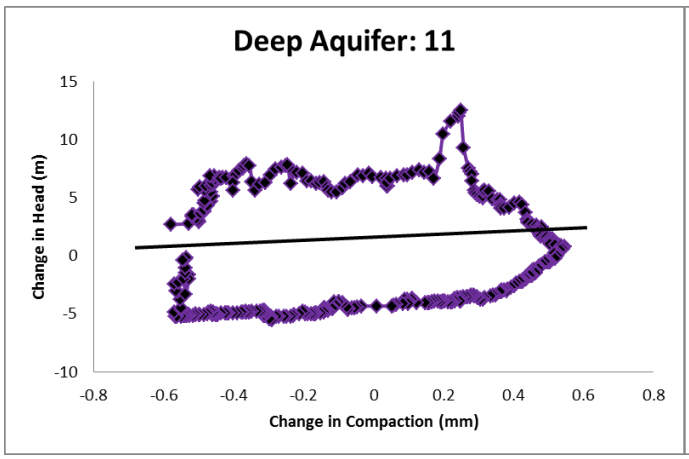
Deep Aquifer: 11
Change in Head (m)
15
10
5
0
-5
-10
-0.8
-0.6
-0.4
-0.2
0
0.2
0.4
0.6
0.8
Change in Compaction (mm)

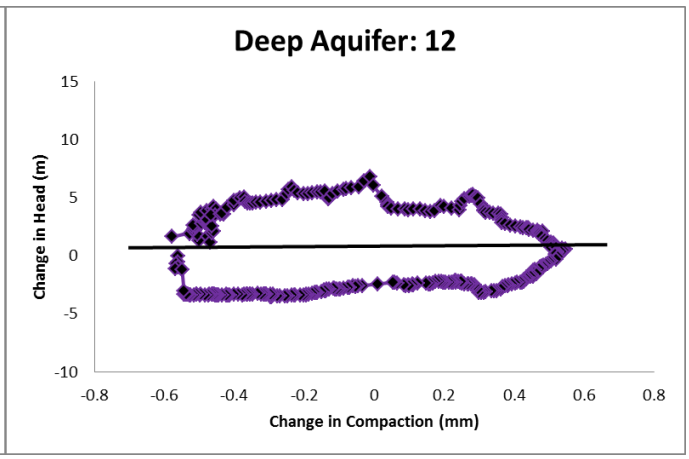
Deep Aquifer: 12
Change in Head (m)
15
10
5
0
-5
-10
-0.8
-0.6
-0.4
-0.2
0
0.2
0.4
0.6
0.8
Change in Compaction (mm)

APPENDIX E

R Code for Time Series Analysis: Maximum Correlation on Seasonal Data Record

```
#shallow aquifer

#record split into year intervals

data95 <- shallow.95
results95 <- ccf(data95$subside, data95$shallow)
cbind(results95$acf,results95$lag)

data96 <- shallow.96
results96 <- ccf(data96$subside, data96$shallow)
cbind(results96$acf,results96$lag)

data97 <- shallow.97
results97 <- ccf(data97$subside, data97$shallow)
cbind(results97$acf,results97$lag)

data98 <- shallow.98
results98 <- ccf(data98$subside, data98$shallow)
cbind(results98$acf,results98$lag)

data99 <- shallow.99
results99 <- ccf(data99$subside, data99$shallow)
cbind(results99$acf,results99$lag)

data00 <- shallow.00
results00 <- ccf(data00$subside, data00$shallow)
cbind(results00$acf,results00$lag)

data01 <- shallow.01
results01 <- ccf(data01$subside, data01$shallow)
cbind(results01$acf,results01$lag)

data02 <- shallow.02
results02 <- ccf(data02$subside, data02$shallow)
cbind(results02$acf,results02$lag)

data03 <- shallow.03
results03 <- ccf(data03$subside, data03$shallow)
cbind(results03$acf,results03$lag)

data04 <- shallow.04
results04 <- ccf(data04$subside, data04$shallow)
```

```
cbind(results04$acf,results04$lag)

data05 <- shallow.05
results05 <- ccf(data05$subside, data05$shallow)
cbind(results05$acf,results05$lag)

data06 <- shallow.06
results06 <- ccf(data06$subside, data06$shallow)
cbind(results06$acf,results06$lag)

data07 <- shallow.07
results07 <- ccf(data07$subside, data07$shallow)
cbind(results07$acf,results07$lag)

#middle aquifer

#record split into year intervals

datam95 <- deep.and.middle.95
resultsm95 <- ccf(datam95$subside, datam95$middle)
cbind(resultsm95$acf, resultsm95$lag)

datam96 <- deep.and.middle.96
resultsm96 <- ccf(datam96$subside, datam96$middle)
cbind(resultsm96$acf, resultsm96$lag)

datam97 <- deep.and.middle.97
resultsm97 <- ccf(datam97$subside, datam97$middle)
cbind(resultsm97$acf, resultsm97$lag)

datam98 <- deep.and.middle.98
resultsm98 <- ccf(datam98$subside, datam98$middle)
cbind(resultsm98$acf, resultsm98$lag)

datam99 <- deep.and.middle.99
resultsm99 <- ccf(datam99$subside, datam99$middle)
cbind(resultsm99$acf, resultsm99$lag)

datam00 <- deep.and.middle.00
resultsm00 <- ccf(datam00$subside, datam00$middle)
cbind(resultsm00$acf, resultsm00$lag)

datam01 <- deep.and.middle.01
resultsm01 <- ccf(datam01$subside, datam01$middle)
cbind(resultsm01$acf, resultsm01$lag)
```

```
datam02 <- deep.and.middle.02
resultsm02 <- ccf(datam02$subside, datam02$middle)
cbind(resultsm02$acf, resultsm02$lag)

datam03 <- deep.and.middle.03
resultsm03 <- ccf(datam03$subside, datam03$middle)
cbind(resultsm03$acf, resultsm03$lag)

datam04 <- deep.and.middle.04
resultsm04 <- ccf(datam04$subside, datam04$middle)
cbind(resultsm04$acf, resultsm04$lag)

datam05 <- deep.and.middle.05
resultsm05 <- ccf(datam05$subside, datam05$middle)
cbind(resultsm05$acf, resultsm05$lag)

datam06 <- deep.and.middle.06
resultsm06 <- ccf(datam06$subside, datam06$middle)
cbind(resultsm06$acf, resultsm06$lag)

datam07 <- deep.and.middle.07
resultsm07 <- ccf(datam07$subside, datam07$middle)
cbind(resultsm07$acf, resultsm07$lag)

#deep aquifer

#record split into year intervals

datad95 <- deep.and.middle.95
resultsd95 <- ccf(datad95$subside, datad95$deep, lag.max = 40)
cbind(resultsd95$acf, resultsd95$lag)

datad96 <- deep.and.middle.96
resultsd96 <- ccf(datad96$subside, datad96$deep, lag.max = 40)
cbind(resultsd96$acf, resultsd96$lag)

datad97 <- deep.and.middle.97
resultsd97 <- ccf(datad97$subside, datad97$deep, lag.max = 40)
cbind(resultsd97$acf, resultsd97$lag)

datad98 <- deep.and.middle.98
resultsd98 <- ccf(datad98$subside, datad98$deep, lag.max = 40)
cbind(resultsd98$acf, resultsd98$lag)

datad99 <- deep.and.middle.99
resultsd99 <- ccf(datad99$subside, datad99$deep, lag.max = 40)
```

```
cbind(resultsd99$acf, resultsd99$lag)

datad00 <- deep.and.middle.00
resultsd00 <- ccf(datad00$subside, datad00$deep, lag.max = 40)
cbind(resultsd00$acf, resultsd00$lag)

datad01 <- deep.and.middle.01
resultsd01 <- ccf(datad01$subside, datad01$deep, lag.max = 40)
cbind(resultsd01$acf, resultsd01$lag)

datad02 <- deep.and.middle.02
resultsd02 <- ccf(datad02$subside, datad02$deep, lag.max = 40)
cbind(resultsd02$acf, resultsd02$lag)

datad03 <- deep.and.middle.03
resultsd03 <- ccf(datad03$subside, datad03$deep, lag.max = 40)
cbind(resultsd03$acf, resultsd03$lag)

datad04 <- deep.and.middle.04
resultsd04 <- ccf(datad04$subside, datad04$deep, lag.max = 40)
cbind(resultsd04$acf, resultsd04$lag)

datad05 <- deep.and.middle.05
resultsd05 <- ccf(datad05$subside, datad05$deep, lag.max = 40)
cbind(resultsd05$acf, resultsd05$lag)

datad06 <- deep.and.middle.06
resultsd06 <- ccf(datad06$subside, datad06$deep, lag.max = 40)
cbind(resultsd06$acf, resultsd06$lag)

datad07 <- deep.and.middle.07
resultsd07 <- ccf(datad07$subside, datad07$deep, lag.max = 40)
cbind(resultsd07$acf, resultsd07$lag)
```

APPENDIX F

Principal Components Analysis: Complete Average Daily Record Set Up

	Depth to water-levels			Compaction
	PZS	PZM	PZD	EXT1
Days of the year	average daily values			

Principal Components Analysis: Daily Values Set Up

Shallow Aquifer (PZS):

	Depth to water-levels				
	1	2	3	4	. . . to 28 days
12 months in each year, 1995-2007	average daily values				

*Completed for middle aquifer (PZM), deep aquifer (PZD), and subsidence (EXT1) records as well.

Principal Components Analysis: Monthly Values Set Up

Shallow Aquifer (PZS):

	Depth to water-levels				
	1	2	3	4	. . . to 12 months
13 years, 1995-2007	average monthly values				

*Completed for middle aquifer (PZM), deep aquifer (PZD), and subsidence (EXT1) records as well.

R code for Principal Components Analysis: Complete Average Daily Record

```
#Total average daily

total.avg.daily <- total.avg.daily
na.exclude(total.avg.daily)
total.avg.daily.nomiss <- na.exclude(total.avg.daily)
```

```
total.avg.daily.prc <- prcomp (total.avg.daily.nomiss, center = TRUE, scale
= FALSE)
total.avg.daily.prc
summary(total.avg.daily.prc)
```

R code for Principal Components Analysis: Daily Values

```
#Daily average deep aquifer

daily.avg.deep95.07 <- daily.avg.deep95.07
daily.avg.deep95.07.prc <- prcomp (daily.avg.deep95.07, center = TRUE, scale = FALSE)
daily.avg.deep95.07.prc
summary (daily.avg.deep95.07.prc)

#Daily average middle aquifer

daily.avg.middle95.07 <- daily.avg.middle95.07
daily.avg.middle95.07.prc <- prcomp (daily.avg.middle95.07, center = TRUE, scale = FALSE)
daily.avg.middle95.07.prc
summary (daily.avg.middle95.07.prc)

#Daily average shallow aquifer

daily.avg.shallow95.07 <- daily.avg.shallow95.07
daily.avg.shallow95.07.prc <- prcomp (daily.avg.shallow95.07, center = TRUE, scale = FALSE)
daily.avg.shallow95.07.prc
summary (daily.avg.shallow95.07.prc)

#Daily average subsidence

daily.avg.subside95.07 <- daily.avg.subside95.07
daily.avg.subside95.07.prc <- prcomp (daily.avg.subside95.07, center = TRUE, scale = FALSE)
daily.avg.subside95.07.prc
summary (daily.avg.subside95.07.prc)
```

R code for Principal Components Analysis: Monthly Values

```
#Monthly average deep aquifer

monthly.avg.deep95.07 <- monthly.avg.deep95.07
monthly.avg.deep95.07.prc <- prcomp (monthly.avg.deep95.07, center = TRUE, scale = FALSE)
monthly.avg.deep95.07.prc
summary (monthly.avg.deep95.07.prc)

#Rotations
```

```
#Varimax Rotation

var.max = varimax(monthly.avg.deep95.07.prc$rotation,normalize = TRUE, eps = 1e-05)
var.max

#Oblimin Rotation

oblimin <- principal(monthly.avg.deep95.07, nfactors = 4, rotation = "oblimin", covar = TRUE)
oblimin

#Monthly average middle aquifer

monthly.avg.middle95.07 <- monthly.avg.middle95.07
monthly.avg.middle95.07.prc <- prcomp (monthly.avg.middle95.07, center = TRUE, scale =
FALSE)
monthly.avg.middle95.07.prc
summary (monthly.avg.middle95.07.prc)

#Rotations

#Varimax Rotation

var.max = varimax(monthly.avg.middle95.07.prc$rotation,normalize = TRUE, eps = 1e-05)
var.max

#Oblimin Rotation

oblimin <- principal(monthly.avg.middle95.07, nfactors = 4, rotation = "oblimin", covar =
TRUE)
oblimin

#Monthly average shallow aquifer

monthly.avg.shallow95.07 <- monthly.avg.shallow95.07
monthly.avg.shallow95.07.prc <- prcomp (monthly.avg.shallow95.07, center = TRUE, scale =
FALSE)
monthly.avg.shallow95.07.prc
summary (monthly.avg.shallow95.07.prc)

#Rotations

#Varimax Rotation

var.max = varimax(monthly.avg.shallow95.07.prc$rotation,normalize = TRUE, eps = 1e-05)
var.max
```

```
#Oblimin Rotation

oblimin <- principal(monthly.avg.shallow95.07, nfactors = 4, rotation = "oblimin", covar =
TRUE)
oblimin

#Monthly average subsidence

monthly.avg.subside95.07 <- monthly.avg.subside95.07
monthly.avg.subside95.07.prc <- prcomp (monthly.avg.subside95.07, center = TRUE, scale =
FALSE)
monthly.avg.subside95.07.prc
summary (monthly.avg.subside95.07.prc)

#Rotations

#Varimax Rotation

var.max = varimax(monthly.avg.subside95.07.prc$rotation,normalize = TRUE, eps = 1e-05)
var.max

#Oblimin Rotation

oblimin <- principal(monthly.avg.subside95.07, nfactors = 4, rotation = "oblimin", covar =
TRUE)
oblimin
```

APPENDIX G

Aquifer horizontal hydraulic conductivity and elastic skeletal specific storage values for the base case (pumping rate proportioned based on aquifer thicknesses) and each 5% iteration determined using AquiferTest Pro (Waterloo Hydrogeology Inc., 2014).

Aquifer	Pumping Rate	Hantush-Jacob (Walton)		Hantush – Storage in Aquitard	
	Q	K_h	S_{ske}	K_h	S_{ske}
	m^3/hr	m/day	1/m	m/day	1/m
Middle	1239.8	188	$6.68x10^{-6}$	184	$6.60x10^{-6}$
	1452.8	220	$7.83x10^{-6}$	216	$7.75x10^{-6}$
	1665.8	252	$8.98x10^{-6}$	248	$8.89x10^{-6}$
	1878.8	284	$1.01x10^{-5}$	280	$1.00x10^{-5}$
	2091.8	317	$1.13x10^{-5}$	313	$1.12x10^{-5}$
	2129.05	323	$1.15x10^{-5}$	319	$1.14x10^{-5}$
Deep	3018.3	69	$1.68x10^{-6}$	66	$1.64x10^{-6}$
	2805.3	64	$1.56x10^{-6}$	61	$1.53x10^{-6}$
	2592.3	59	$1.44x10^{-6}$	57	$1.41x10^{-6}$
	2379.3	54	$1.32x10^{-6}$	52	$1.29x10^{-6}$
	2166.3	49	$1.20x10^{-6}$	47	$1.17x10^{-6}$
	2129.05	48	$1.18x10^{-6}$	46	$1.15x10^{-6}$

Hantush-Jacob (Walton) method calculation for hydraulic resistance (Waterloo Hydrogeology Inc., 2014):

$$c = \frac{b'}{K_v'} = \frac{32\ m}{2.66x10^{-5}\ \frac{m}{d}} = 1203007.5\ days = 2.89x10^{7}\ hrs$$

b' = thickness of deep aquitard, $32\ m$

K_v' = deep aquitard vertical hydraulic conductivity, $2.66x10^{-5}\ \frac{m}{d}$

Hantush – Storage in Aquitard method calculation of adequate period of time for the pumping test (Waterloo Hydrogeology Inc., 2014):

$$t < \frac{S'b'}{10K_v'} < \frac{1.04x10^{-4} * 32\ m}{10 * 2.66x10^{-5}\ \frac{m}{d}} < 12.5\ days$$

b' = thickness of deep aquitard, $32\ m$

K_v' = deep aquitard vertical hydraulic conductivity, $2.66x10^{-5}\ \frac{m}{d}$

S' = deep aquitard storage coefficient, $1.04x10^{-4}$

Proportioning the pumping rate between the middle and deep aquifers based on the aquifer thicknesses.

Aquifer	**Thickness**	**Pumping Rate**
	m	m^3/hr
Middle	24.4	1239.8
Deep	59.4	3018.3
Total	**83.8**	**4258.1**

APPENDIX H

Aquitard stress-strain slopes, storage coefficients, and elastic specific storage values for 12 cycles as well as averaged values, standard deviations, and margin of errors.

	Shallow Slope	Storage Coefficient	Specific Storage (1/m)	Middle Slope	Storage Coefficient	Specific Storage (1/m)	Deep Slope	Storage Coefficient	Specific Storage (1/m)
	8000.0	1.25E-04	7.74E-06	10000.0	1.00E-04	4.10E-06	9090.9	1.10E-04	1.85E-06
	7272.7	1.38E-04	8.51E-06	12631.6	7.92E-05	3.25E-06	10000.0	1.00E-04	1.68E-06
	8421.1	1.19E-04	7.35E-06	11818.2	8.46E-05	3.47E-06	8333.3	1.20E-04	2.02E-06
	11250.0	8.89E-05	5.50E-06	11764.7	8.50E-05	3.49E-06	8333.3	1.20E-04	2.02E-06
	12727.3	7.86E-05	4.86E-06	12500.0	8.00E-05	3.28E-06	8750.0	1.14E-04	1.92E-06
	15000.0	6.67E-05	4.13E-06	8888.9	1.12E-04	4.61E-06	6818.2	1.47E-04	2.47E-06
	12941.2	7.73E-05	4.78E-06	8888.9	1.12E-04	4.61E-06	5555.6	1.80E-04	3.03E-06
	13750.0	7.27E-05	4.50E-06	11428.6	8.75E-05	3.59E-06	7692.3	1.30E-04	2.19E-06
	12381.0	8.08E-05	5.00E-06	11764.7	8.50E-05	3.49E-06	1388.9	7.20E-04	1.21E-05
	16250.0	6.15E-05	3.81E-06	10000.0	1.00E-04	4.10E-06	6250.0	1.60E-04	2.69E-06
	10476.2	9.55E-05	5.91E-06	6666.7	1.50E-04	6.15E-06	4411.8	2.27E-04	3.81E-06
	11111.1	9.00E-05	5.57E-06	3200.0	3.13E-04	1.28E-05	-	-	-
Average	11631.7167	9.11E-05	5.64E-06	9962.69	1.16E-04	4.75E-06	6965.85	1.93E-04	3.25E-06
Standard Deviation	2908.47	2.40E-05	1.49E-06	2772.49	6.51E-05	2.67E-06	2476.31	1.78E-04	3.00E-06
Margin of Error	1953.94	1.53E-05	9.45E-07	1761.56	4.14E-05	1.70E-06	1663.61	1.20E-04	2.02E-06

APPENDIX I

Individual year-long and average seasonal signal aquitard lag times determined by maximum correlation.

Year	Shallow Aquifer	Middle Aquifer	Deep Aquifer
		days	
1995	0	0	15
1996	19	19	34
1997	12	18	34
1998	6	22	35
1999	3	21	34
2000	5	16	34
2001	3	15	30
2002	3	10	28
2003	3	22	36
2004	0	19	35
2005	0	15	32
2006	0	14	28
Average	4.5	15.9	31.3
Standard Deviation	5.7	6.2	5.8
Margin of Error	3.6	3.9	3.7

APPENDIX J

Deep Aquifer: Daily Principal Components Analysis Results

For brevity, only six of the 28 principal components are listed from the results. The x-number column refers to the day in a 28-day long month.

	PC1	PC2	PC3	PC4	PC5	PC6
X1	-0.1877396	-0.38342138	0.215491501	0.42250873	-0.31303458	0.170129973
X2	-0.1861655	-0.31687531	0.186299787	0.26773652	-0.24505016	0.117012112
X3	-0.1876070	-0.27095698	0.152700171	0.13207296	-0.11843677	-0.091622726
X4	-0.1876949	-0.24617527	0.127966339	-0.03663972	0.22035859	-0.168446060
X5	-0.1871118	-0.22431842	0.110651005	-0.04754486	0.32379292	-0.264494755
X6	-0.1879370	-0.18467594	0.067279567	-0.07747912	0.32429256	-0.214550572
X7	-0.1881377	-0.16206287	-0.007032932	-0.13732568	0.24109038	-0.077816242
X8	-0.1881812	-0.13410024	-0.026802596	-0.15987526	0.19570298	0.200260815
X9	-0.1877651	-0.10319160	-0.056997200	-0.21171499	0.17630461	0.396501407
X10	-0.1874998	-0.09005419	-0.056447847	-0.20369436	0.13663405	0.303780245
X11	-0.1884445	-0.06622412	-0.060809136	-0.19056807	-0.01048429	-0.048544472
X12	-0.1883539	-0.04377777	-0.121700061	-0.25133062	-0.21892641	-0.215391275
X13	-0.1876521	-0.04260130	-0.154311440	-0.26319553	-0.37773731	-0.220111528
X14	-0.1877498	-0.02301803	-0.166482894	-0.27687713	-0.34380847	-0.074994325
X15	-0.1879414	0.00753509	-0.208656759	-0.15999223	-0.24128683	-0.006894914
X16	-0.1886428	0.02894635	-0.253313492	0.05759723	-0.02842130	0.202922789
X17	-0.1891203	0.05930154	-0.311311469	0.12905891	0.05973499	0.310307751
X18	-0.1897331	0.08845776	-0.306928334	0.23522673	0.04623748	0.069401119
X19	-0.1906781	0.11253879	-0.266126236	0.30997543	0.09386693	-0.062612235
X20	-0.1910598	0.15171297	-0.246136764	0.28060127	0.12096347	-0.136627659
X21	-0.1905337	0.17794222	-0.058636332	0.19514089	0.09320653	-0.192304339
X22	-0.1898094	0.19727706	0.047176105	0.09369862	0.05535813	-0.131342321
X23	-0.1906467	0.21486899	0.126520734	0.05984984	-0.03447714	-0.269096154
X24	-0.1909993	0.21740646	0.164726697	0.03506048	-0.04440401	-0.122990060
X25	-0.1909440	0.22465461	0.215403315	0.01720668	-0.05779940	0.009667945
X26	-0.1906725	0.23527090	0.275634095	-0.04891978	-0.04822626	0.098353263
X27	-0.1909668	0.25705243	0.297599365	-0.08496896	-0.05727319	0.233248799
X28	-0.1915486	0.28044598	0.308507357	-0.09644120	0.04718763	0.187787253

Importance of components:

	PC1	PC2	PC3	PC4	PC5	PC6
Standard deviation	42.8809	3.47919	1.30565	0.88581	0.59755	0.48868
Proportion of Variance	0.9912	0.00653	0.00092	0.00042	0.00019	0.00013

```
Cumulative Proportion   0.9912 0.99776 0.99868 0.99910 0.99929 0.99942
```

Deep Aquifer: Monthly Principal Components Analysis Results

For brevity, only six of the 12 principal components are listed from the results. The x-number column refers to the month in the year.

	PC1	PC2	PC3	PC4	PC5	PC6
X1	-0.2600411	0.20088690	0.31554099	-0.51616059	0.01898453	0.19090120
X2	-0.2619930	0.13681101	0.35973292	-0.17162534	-0.01592002	-0.05537411
X3	-0.2583746	0.15696405	0.33643111	-0.07760523	-0.12054571	-0.15392140
X4	-0.2584584	0.18862439	0.32848426	0.18870362	-0.31910127	-0.18295112
X5	-0.2862668	0.49225389	-0.04556402	0.65409235	0.09929301	0.37469994
X6	-0.2852771	0.21419262	-0.31078526	-0.26147091	0.52878115	0.02329875
X7	-0.3026126	0.18713809	-0.38495455	-0.12644630	0.21506225	-0.21739499
X8	-0.3085411	-0.05021531	-0.26649564	-0.02294851	-0.26153827	-0.54654500
X9	-0.3195922	-0.19150665	-0.36594137	-0.21150094	-0.54145511	0.57577631
X10	-0.3176339	-0.23804005	-0.08154501	0.17974303	-0.11794195	-0.13230637
X11	-0.3029062	-0.42765964	0.02333271	0.26592721	0.15758247	-0.12096695
X12	-0.2920509	-0.52796315	0.30159200	0.04488572	0.38339331	0.22968737

```
Importance of components:
                          PC1     PC2     PC3     PC4     PC5     PC6
Standard deviation     27.0158 3.05278 2.29848 1.32567 1.03203 0.58794
Proportion of Variance  0.9755 0.01246 0.00706 0.00235 0.00142 0.00046
Cumulative Proportion   0.9755 0.98796 0.99502 0.99737 0.99879 0.99925
```

Deep Aquifer: Rotated Monthly Principal Components Analysis Results

The x-number column refers to the month in the year.

Varimax Rotation Results

```
Loadings:
    PC1 PC2 PC3 PC4 PC5 PC6 PC7 PC8 PC9 PC10 PC11 PC12
X1                          -1
X2                                   1
X3                                            -1
X4   1
X5               1
```

```
X6                   1
X7                             1
X8                      -1
X9          -1
X10                                       1
X11                           1
X12     -1
```

	PC1	PC2	PC3	PC4	PC5	PC6
SS loadings	1.000	1.000	1.000	1.000	1.000	1.000
Proportion Var	0.083	0.083	0.083	0.083	0.083	0.083
Cumulative Var	0.083	0.167	0.250	0.333	0.417	0.500

	PC7	PC8	PC9	PC10	PC11	PC12
SS loadings	1.000	1.000	1.000	1.000	1.000	1.000
Proportion Var	0.083	0.083	0.083	0.083	0.083	0.083
Cumulative Var	0.583	0.667	0.750	0.833	0.917	1.000

Oblimin Rotation Results: Pattern Matrix

Unstandardized loadings:

	PC2	PC3	PC1	PC4	h2	u2	H2	U2
X1	3.9	4.9	3.2	-0.63	51	0.078	1.00	0.00154
X2	4.2	4.9	3.1	-0.18	51	0.029	1.00	0.00058
X3	4.0	4.8	3.1	-0.05	50	0.050	1.00	0.00100
X4	4.0	4.9	3.2	0.30	50	0.177	1.00	0.00355
X5	3.6	5.3	4.5	0.99	63	0.080	1.00	0.00128
X6	4.1	4.5	4.8	-0.27	60	0.376	0.99	0.00618
X7	4.5	4.7	5.1	-0.09	68	0.109	1.00	0.00160
X8	5.2	4.5	4.8	0.00	70	0.262	1.00	0.00373
X9	5.7	4.3	5.0	-0.27	76	0.431	0.99	0.00566
X10	5.8	4.5	4.4	0.24	74	0.081	1.00	0.00109
X11	6.1	4.1	3.8	0.31	69	0.080	1.00	0.00116
X12	6.2	4.1	3.1	-0.01	65	0.217	1.00	0.00331

	PC2	PC3	PC1	PC4
SS loadings	284.46	259.27	200.69	1.8
Proportion Var	0.38	0.35	0.27	0.0
Cumulative Var	0.38	0.73	0.99	1.0
Proportion Explained	0.38	0.35	0.27	0.0
Cumulative Proportion	0.38	0.73	1.00	1.0

Standardized loadings:

	item	PC2	PC3	PC1	PC4	h2	u2
X1	1	0.55	0.69	0.45	-0.09	1.00	0.00154

X2	2	0.58	0.69	0.44	-0.03	1.00	0.00058
X3	3	0.57	0.69	0.44	-0.01	1.00	0.00100
X4	4	0.56	0.69	0.45	0.04	1.00	0.00355
X5	5	0.46	0.67	0.56	0.12	1.00	0.00128
X6	6	0.53	0.58	0.61	-0.03	0.99	0.00618
X7	7	0.54	0.56	0.62	-0.01	1.00	0.00160
X8	8	0.62	0.54	0.57	0.00	1.00	0.00373
X9	9	0.65	0.49	0.57	-0.03	0.99	0.00566
X10	10	0.68	0.53	0.51	0.03	1.00	0.00109
X11	11	0.73	0.49	0.46	0.04	1.00	0.00116
X12	12	0.77	0.51	0.38	0.00	1.00	0.00331

	PC2	**PC3**	**PC1**	**PC4**
SS loadings	4.47	4.32	3.15	0.03
Proportion Var	0.37	0.36	0.26	0.00
Cumulative Var	0.37	0.73	0.99	1.00
Cum. factor Var	0.37	0.73	1.00	1.00

Mean item complexity = 2.7
Test of the hypothesis that 4 components are sufficient.

The root mean square of the residuals (RMSR) is 0.08
with the empirical chi square 11.12 with prob < 0.99

Fit based upon off diagonal values = 1